



Weld Design, Testing, and Assessment Procedures for High-strength Pipelines Curved Wide Plate Tests

Final Report 277-T-09

For Project

Weld Design, Testing, and Assessment Procedures for High Strength Pipelines

Prepared for the

Design, Materials, and Construction Technical Committee of
Pipeline Research Council International, Inc.
Project MATH-1 Catalog No. L5XXXX

and

U.S. Department of Transportation
Pipeline and Hazardous Materials Safety Administration
Office of Pipeline Safety
Agreement Number DTPH56-07-T-000005

Prepared by

Timothy Weeks, J. David McColskey and Mark Richards
National Institute of Standards and Technology

Assisted by

Yong-Yi Wang/CRES, Honggang (Michael) Zhou—Center for Reliable Energy Systems
Bill Tyson, Jim Gianetto—CANMET Materials Technology Laboratory
Marie Quintana—Lincoln Electric Company

September 2011

This research was funded in part under the Department of Transportation, Pipeline and Hazardous Materials Safety Administration's Pipeline Safety Research and Development Program. The views and conclusions contained in this document are those of the authors and should not be interpreted as representing the official policies, either expressed or implied, of the Pipeline and Hazardous Materials Safety Administration, or the U.S. Government. Contribution of an agency of the U.S. government, not subject to copyright



Catalog No. L5XXXX

Weld Design, Testing, and Assessment Procedures for High-strength Pipelines Curved Wide Plate Tests

Final Report 277-T-09

For Project

Weld Design, Testing, and Assessment Procedures for High Strength Pipelines

Prepared for the

Design, Materials, and Construction Technical Committee of Pipeline Research Council International, Inc.
Project MATH-1 Catalog No. L5XXXX

and

U.S. Department of Transportation
Pipeline and Hazardous Materials Safety Administration
Office of Pipeline Safety
Agreement Number DTPH56-07-T-000005

Prepared by

Timothy Weeks, J. David McColskey and Mark Richards
National Institute of Standards and Technology

Assisted by

Center for Reliable Energy Systems
CANMET Materials Technology Laboratory
Yong-Yi Wang/CRES, Honggang (Michael) Zhou—Center for Reliable Energy Systems
Bill Tyson, Jim Gianetto— CANMET Materials Technology Laboratory
Marie Quintana—Lincoln Electric Company

September 2011

Version	Date of Last Revision	Date of Uploading	Comments
1.0	April 12, 2011	April 12, 2011	
Final	September 1, 2011	December 1, 2011	

This report is furnished to Pipeline Research Council International, Inc. (PRCI) under the terms of PRCI contract [277-PR-348-074512], between PRCI and the MATH-1 contractors:

- Electricore (prime contractor),
- Center for Reliable Energy Systems, CANMET, NIST, and The Lincoln Electric Company (sub-contractors).

The contents of this report are published as received from the MATH-1 contractor and subcontractors. The opinions, findings, and conclusions expressed in the report are those of the authors and not necessarily those of PRCI, its member companies, or their representatives. Publication and dissemination of this report by PRCI should not be considered an endorsement by PRCI of the MATH-1 contractor and subcontractors, or the accuracy or validity of any opinions, findings, or conclusions expressed herein.

In publishing this report, PRCI and the MATH-1 contractors make no warranty or representation, expressed or implied, with respect to the accuracy, completeness, usefulness, or fitness for purpose of the information contained herein, or that the use of any information, method, process, or apparatus disclosed in this report may not infringe on privately owned rights. PRCI and the MATH-1 contractors assume no liability with respect to the use of, or for damages resulting from the use of, any information, method, process, or apparatus disclosed in this report. By accepting the report and utilizing it, you agree to waive any and all claims you may have, resulting from your voluntary use of the report, against PRCI and the MATH-1 contractors.

Pipeline Research Council International Catalog No. L5XXXX

PRCI Reports are Published by Technical Toolboxes, Inc.

3801 Kirby Drive, Suite 520
Houston, Texas 77098
Tel: 713-630-0505
Fax: 713-630-0560
Email: info@ttoolboxes.com

PROJECT PARTICIPANTS

PROJECT TEAM MEMBER	COMPANY AFFILIATION	PROJECT TEAM MEMBER	COMPANY AFFILIATION
Arti Bhatia	Alliance	Jim Costain	GE
Jennifer Klementis	Alliance	Gilmar Batista	Petrobras
Roger Haycraft	Boardwalk	Marcy Saturno de Menezes	Petrobras
David Horsley	BP	Dave Aguiar	PG&E
Mark Hudson	BP	Ken Lorang	PRCI
Ron Shockley	Chevron	Maslat Al-Waranbi	Saudi Aramco
Sam Mishael	Chevron	Paul Lee	SoCalGas
David Wilson	ConocoPhillips	Alan Lambeth	Spectra
Satish Kulkarni	El Paso	Robert Turner	Stupp
Art Meyer	Enbridge	Gilles Richard	TAMSA
Bill Forbes	Enbridge	Noe Mota Solis	TAMSA
Scott Ironside	Enbridge	Philippe Darcis	TAMSA
Sean Keane	Enbridge	Dave Taylor	TransCanada
Laurie Collins	Evraz	Joe Zhou	TransCanada
David de Miranda	Gassco	Jason Skow	TransGas
Adriaan den Herder	Gasunie	Ernesto Cisneros	Tuberia Laguna
Jeff Stetson	GE	Vivek Kashyap	Welpsun
		Chris Brown	Williams

CORE RESEARCH TEAM	
RESEARCHER	COMPANY AFFILIATION
Yaoshan Chen	Center for Reliable Energy Systems
Yong-Yi Wang	Center for Reliable Energy Systems
Ming Liu	Center for Reliable Energy Systems
Dave Fink	Lincoln Electric Company
Marie Quintana	Lincoln Electric Company
Vaidyanath Rajan	Lincoln Electric Company
Joe Daniel	Lincoln Electric Company
Radhika Panday	Lincoln Electric Company
James Gianetto	CANMET Materials Technology Laboratory
John Bowker	CANMET Materials Technology Laboratory
Bill Tyson	CANMET Materials Technology Laboratory
Guowu Shen	CANMET Materials Technology Laboratory
Dong Park	CANMET Materials Technology Laboratory
Timothy Weeks	National Institute of Standards and Technology
Mark Richards	National Institute of Standards and Technology
Dave McColskey	National Institute of Standards and Technology
Enrico Lucon	National Institute of Standards and Technology
John Hammond	Consultant Metallurgist & Welding Engineer

This Page Intentionally Left Blank

FINAL REPORT STRUCTURE

Focus Area 1 - Update of Weld Design, Testing, and Assessment Procedures for High Strength Pipelines		
Report #	Description	Lead Authors
277-T-01	Background of Linepipe Specifications	CRES/CANMET
277-T-02	Background of All-Weld Metal Tensile Test Protocol	CANMET/Lincoln
277-T-03	Development of Procedure for Low-Constraint Toughness Testing Using a Single-Specimen Technique	CANMET/CRES
277-T-04	Summary of Publications: Single-Edge Notched Tension SE(T) Tests	CANMET
277-T-05	Small Scale Tensile, Charpy V-Notch, and Fracture Toughness Tests	CANMET/NIST
277-T-06	Small Scale Low Constraint Fracture Toughness Test Results	CANMET/NIST
277-T-07	Small Scale Low Constraint Fracture Toughness Test Discussion and Analysis	CANMET/NIST
277-T-08	Summary of Mechanical Properties	CANMET
277-T-09	Curved Wide Plate Tests	NIST/CRES
277-T-10	Weld Strength Mismatch Requirements	CRES/CANMET
277-T-11	Curved Wide Plate Test Results and Transferability of Test Specimens	CRES/CANMET
277-S-01	Summary Report 277 Weld Design, Testing, and Assessment Procedures for High Strength Pipelines	CRES

Focus Area 2 - Development of Optimized Welding Solutions for X100 Linepipe Steel		
Report #	Description	Lead Authors
278-T-01	State of The Art Review	Lincoln
278-T-02	Material Selection, Welding and Weld Monitoring	Lincoln/CANMET
278-T-03	Microstructure and Hardness Characterization of Girth Welds	CANMET/Lincoln
278-T-04	Microstructure and Properties of Simulated Weld Metals	CANMET/Lincoln
278-T-05	Microstructure and Properties of Simulated Heat Affected Zones	CANMET/Lincoln
278-T-06	Essential Welding Variables	Lincoln/CANMET
278-T-07	Thermal Model for Welding Simulations	CRES/CANMET
278-T-08	Microstructure Model for Welding Simulations	CRES/CANMET
278-T-09	Application to Other Processes	Lincoln/CANMET
278-S-01	Summary Report 278 Development of Optimized Welding Solutions for X100 Line Pipe Steel	Lincoln

EXECUTIVE SUMMARY

A variety of mechanical property tests are performed in the design, construction and maintenance phase of a pipeline. Most of the tests are performed by use of small-scale specimens with size typically in the range of a few inches to tens of inches (1 in = 25.4 mm). There are numerous test labs capable of performing most small-scale tests. These tests can be performed effectively under a variety of conditions, *e.g.*, test temperature, strain rate, and loading configuration. More importantly, most routine small-scale tests are performed in accordance with national and international standards, ensuring the consistency of testing procedures.

To confirm pipeline designs and validate material performance, it is desirable to test girth welds under realistic service conditions. Full-scale tests can incorporate certain realistic features that small-scale specimens cannot. However, these tests can be time-consuming and expensive to conduct. Very few labs can perform the tests, even with months of start-up and preparation time. There are no generally accepted, consistent test procedures among different test labs. The data acquisition and post-processing may differ from lab to lab, creating difficulties in data comparison. Full-scale tests can only be performed under selected conditions as a supplemental tool to the small-scale tests. The amount of resources and time required to conduct such tests prevent them from becoming routine tests.

Situated in the middle of the specimen size scale is a medium-scale test, such as curved- wide-plate (CWP) test. CWP tests are more difficult to conduct than small-scale tests. However they are considerably easier to conduct than full-scale tests. Much of the information needed from full-scale tests can be obtained from CWP tests. Several commercial labs are set up to conduct CWP tests on a routine basis.

The work described in this report focuses on the development of test procedures and instrumentation requirements for curved-wide-plate (CWP) tests. The results of this work can be used for:

- (1) Developing a test methodology to measure the physical response of a finite-length surface-breaking flaw to axial loads applied to a girth welded linepipe section,
- (2) Determining the appropriate instrumentation to fully characterize the global stress/strain response of the CWP specimen during loading,
- (3) Evaluating the applicability of the test methodology for sub-ambient temperatures, and
- (4) Developing a standardized test procedure for CWP testing with a wide range of test parameters.

TABLE OF CONTENTS

EXECUTIVE SUMMARY	vii
TABLE OF CONTENTS.....	viii
LIST OF FIGURES	x
LIST OF TABLES.....	xii
1 INTRODUCTION AND BACKGROUND	1
1.1 BACKGROUND	1
1.2 IMPACT	2
1.3 OBJECTIVE	3
1.4 SCOPE OF THIS REPORT.....	3
1.5 TEST MATRIX	3
2 CURVED-WIDE-PLATE SPECIMEN.....	5
2.1 GENERAL CONSIDERATIONS	5
2.2 MATERIAL.....	5
2.3 SPECIMEN GEOMETRY	5
3 SPECIMEN PREPARATION	9
3.1 SPECIMEN EXTRACTION PLAN.....	9
3.2 MACHINING	9
3.3 SHIPPING CONSIDERATIONS.....	9
3.4 SURFACE PREPARATIONS.....	11
3.5 NOTCHING.....	11
3.6 FATIGUE PRE-CRACKING.....	14
3.7 WELDING END-TABS	22
4 INSTRUMENTATION	24
4.1 INSTRUMENTATION PLAN.....	24
4.2 PHOTO-ELASTIC FILM.....	25
4.3 STRAIN GAGES.....	26
4.4 LINEAR VARIABLE DIFFERENTIAL TRANSFORMERS.....	27
4.5 CRACK MOUTH OPENING DISPLACEMENT (CMOD) GAUGES	27
4.6 THERMOCOUPLES.....	28
4.7 CALIBRATIONS	28
4.8 DATA ACQUISITION.....	30
5 TEST EQUIPMENT	33
5.1 LOAD FRAME.....	33
5.2 SPECIMEN GRIPS	33
5.3 ENVIRONMENTAL CHAMBER	33
6 TEST PROCEDURE	35
6.1 PHYSICAL MEASUREMENTS	35
6.2 SPECIMEN INSTALLATION.....	36
6.3 INSTRUMENTATION PREPARATIONS	37
6.4 PRE-LOAD.....	38
6.5 COOLING	38
6.6 TEST EXECUTION.....	38
6.7 POST-TEST ACTIVITIES.....	40
7 SPECIMEN ANALYSIS	42
7.1 DATA VERIFICATION	42

7.2	RESIDUAL FLAW GEOMETRY	43
7.3	SPECIMEN DISPOSITION	49
8	DISCUSSION	49
8.1	TOPICAL REPORT COMPLETION	49
8.2	DISCUSSIONS.....	49
8.3	ANOMALIES	50
8.4	TEST METHOD STANDARDIZATION.....	51
8.5	FUTURE WORK.....	51
9	CONCLUSION.....	51
10	REFERENCES	52

LIST OF FIGURES

Figure 1. Dimensioned schematic of CWP specimen from 19.1 mm thick linepipe section, for pipe A. (dimensions in mm).....	7
Figure 2. Placement and profile of the flaws introduced in the CWP specimen. This illustration is based on a 3 mm x 50 mm flaw. The lines in the figure represent the fatigue crack, the end of the second EDM step and the end the end of the first EDM step, from top to bottom, respectively.....	8
Figure 3. Specimens designated for HAZ testing were notched according to this schematic. The initial crack depth, a_o includes the depth of the EDM starter notch and the fatigue pre-crack depth.	9
Figure 4. First shipment of specimens received at NIST. The first two specimens were base metal specimens without girth welds.	10
Figure 5. Shipping crate designed and fabricated at Lincoln Electric for shipping CWP specimens between NIST and Lincoln Electric.	10
Figure 6. Photograph of the ID surface of a specimen, showing the minimal surface changes necessary to prepare the surface for instrumentation. Strain gages and LVDTs are installed on the specimen in this photo. This was a room-temperature test, so thermocouples are absent; however, the area necessary to install thermocouples was very small.....	11
Figure 7. Photograph of the slitting saw head close to the ID surface of the base metal specimen	12
Figure 8. An exaggerated illustration showing the plate misalignment, the EDM reference surface and a notch placed in the weld. This diagram also illustrates the datum for initial crack depth, a_o , measurement.....	13
Figure 9. Cross-section diagram describing the notch depths and relative geometry of the EDM starter notch with respect to the final flaw depth for the 3 mm x 50 mm flaw. All depths given in mm with the included angle in degrees.	14
Figure 10. Schematic of contoured outer-span loading supports (blue) and straight-roller inner-span (green) loading arrangement used in four-point bending fatigue pre-cracking of curved-wide-plates [6].	15
Figure 11. Offset compliance versus optically measured crack depth data for CWP notch geometries in base metal.....	19
Figure 12. Compliance versus the number of cycles plot for two starter notch geometries.....	20
Figure 13. SEM image of fatigue pre-crack fracture surface showing fatigue marker bands. Initial EDM notch geometry was 5.4 mm deep by 28.3 mm wide [6].	20
Figure 14. Centroid positions of the gauge section of the CWP specimen of the two pipe geometries (top) pipe A (19.1 mm thick) and (bottom) pipe B (14.20 mm thick). Units given in mm.	23
Figure 15. Schematic diagram of the instrumentation layout for the CWP testing. Dimensions are given in mm.	25
Figure 16. Outside diameter side of the specimen showing the installation of the photoelastic film covered by the polarizing sheets on the specimen. Cut-outs in the photoelastic and polarizing film allowed the installation of the LVDTs and strain gages.	26
Figure 17. Schematic of the engagement of the clip gauge teeth in the notch of the specimen.	27

Figure 18. Inside-diameter side of the specimen, showing the installation of the CMOD gauges in the notch.....	28
Figure 19. Test frame showing the specimen loading configuration. The location of the upper crosshead, testing load cell, calibration load cell (not present during normal testing), frame support columns, clevis grips, the calibration block and the hydraulic actuator are indicated.....	30
Figure 20. Schematic of the data flow and connection diagram for the CWP tests.	32
Figure 21. The empty environmental chamber (left) and an installed CWP specimen, with the environmental chamber between the grips prepared for testing (right). The chamber is supported by rollers attached to a tracked aluminum frame, allowing the chamber to easily slide in and out of the way of the load line of the frame.	34
Figure 22. Bottom cooling blocks installed on a CWP specimen.	35
Figure 23. Photograph taken during the specimen installation process. The movable counter-balance strong-back was supported by the overhead crane, allowing adequate reach into the test frame, where the overhead crane had no direct access, because of the crosshead.....	37
Figure 24. Graphical representation of the unloading and reloading triggers used after the yield point in the test. The circles represent the areas where the limits switch from load limits to displacement limits (left circle) and then back (right circle).....	39
Figure 25. Load-displacement and CMOD-displacement relation (Specimen ID: CWP-11).....	40
Figure 26. Schematic of a sectioned specimen after testing. The vertical sectioning planes shown in red are for EDM slicing. The horizontal sectioning plane was back cut with a band saw to make it easier to liberate the fracture surface in three-point bending.....	42
Figure 27. Photographs of the crack mouth profile were taken of each specimen to map the profile and quantify the residual opening. This example is from specimen CWP-12.....	44
Figure 28. Fractographs of each specimen were taken to measure the initial and final crack depths, and to determine the crack propagation shape. This example is from specimen CWP-19.....	45
Figure 29. Measured crack depth vs. predicted initial crack depth for all CWP specimens. The data show an excellent predictive capability in the fatigue pre-cracking procedure. The tolerance bands represent an error of ± 0.25 mm.....	46
Figure 30. Metallography was performed on each specimen to document the location of the notch and pre-crack with respect to the weld structure. This macro-scale view was obtained with a high-resolution flat-bed scanner. This example is from specimen CWP-2.....	48
Figure 31. Metallography was performed on each specimen to document the location of the notch and pre-crack with respect to the weld structure. These low-power micrographs were obtained with a high-resolution CMOS camera attached to an optical microscope. This example is from specimen CWP-5.	49

LIST OF TABLES

Table 1. CWP test matrix.....	4
Table 2. Nominal dimensions of CWP test specimens.....	6
Table 3. Nominal surface-breaking flaw geometries of CWP test specimens.....	8
Table 4. Nominal notch geometries for 0.6 mm pre-crack requirements.....	14
Table 5. Stress intensity factor and typical fatigue pre-crack stress intensity factor amplitude levels.....	18
Table 6. Offset Compliance versus Crack Depth Correlation Slope Values.....	22
Table 7. End-tab welding process parameters.....	23
Table 8. Measurements from fractographs.....	47

1 INTRODUCTION AND BACKGROUND

1.1 BACKGROUND

A variety of mechanical property tests are performed in the design, construction and maintenance phase of a pipeline. The linepipe steels are often qualified by tests such as tensile, Charpy impact and drop weight tear tests (DWTT). Girth welding procedure qualification requires at least cross-weld tensile, side bend and/or root bend, and/or nick-break tests. For welding procedures qualified for alternative flaw acceptance criteria (alternatively termed ECA, or engineering critical assessment), fracture toughness tests and/or Charpy impact tests are required. These tests are generally referred to as small-scale tests. The size of those specimens is typically in the range of a few inches to tens of inches (1 in = 25.4 mm). The specimens are usually small enough to be handled manually without the assistance of lifting equipment. There is a wide selection of test labs for most small-scale tests. These tests can be performed effectively under a variety of conditions, *e.g.*, test temperature, strain rate, and loading configuration. More importantly, most routine small-scale tests are performed in accordance with national and international standards, so the consistency of testing procedures is usually very good. Having consistent, transparent, and robust test standards ensures that the differences in the test data are attributable to material behavior, not testing procedures themselves.

To confirm pipeline designs and validate material performance, it is desirable to test girth welds under realistic service conditions in full scale. Full-scale tests can incorporate certain realistic features that small-scale specimens cannot. These features include, but are not limited to, finite-length surface-breaking flaws, high-low misalignment of the welded-joint, and internal pressure. Full-scale tests may be necessary to qualify the impact of those features. However, these tests present their own challenges and pitfalls, such as the following.

- (1) The tests can take months to prepare.
- (2) The tests are very expensive to conduct.
- (3) There is a limited number of test frames capable of handling large-diameter pipes. Sometimes test frames have to be purposely built. These frames may have to be decommissioned when the tests are completed, as they take up too much space.
- (4) Certain test conditions, such as low temperature tests, are difficult to achieve uniformly for very large specimens.
- (5) There are no generally accepted consistent test procedures among different test labs. The data acquisition and post-processing may differ from lab to lab, creating difficulties in data comparison.

In summary, full-scale tests can be performed only under selected conditions as a supplemental tool to the small-scale tests. The amount of resources and time required to conduct such tests prevent them from becoming routine tests.

Situated in the middle of the specimen size scale is the medium-scale test, such as curved- wide plate test. The CWP specimen is a curved piece of pipe with a nominal gauge width of 200 mm to 450 mm (8 in to 18 in) and length in the range of four to six times the gauge width. A girth weld is located in the mid-length of the specimen. In most cases, an artificial machine notch or fatigue-sharpened flaw is introduced in the weld centerline or heat-affected zone. The

deformation and load are monitored during the tests while the specimen is pulled longitudinally until failure or reaching certain predetermined conditions, such as passing the maximum load.

CWP tests have been used for the characterization of girth weld performance for many years [1,2]. More recently, wide-plate tests have become one of the most recognized tools for the determination of girth weld tensile strain capacity. Many organizations now have CWP testing capabilities, including the University of Ghent, C-FER, Stress Engineering Services, National Institute of Standards and Technology (NIST), Evraz, JFE Steel Corporation, Nippon Steel Corporation and POSCO.

In order to use test specimens of various scales effectively, one has to understand their useful features and limits. One of the critical questions is the transferability of test results, *i.e.*, how the test results from one scale of test specimen can be correlated to the results of another scale of test specimen. This question is not easy to answer.

- Ideally, tests of different scales can be performed to evaluate the transferability of results. The reality is significantly more challenging. Material properties often have local variations, particularly in welds and HAZ. The test results from nominally the same material and the same test conditions can vary due to those local variations. It is well documented from large-scale tests that flaws under “nominally identical conditions” can behave quite differently [3]. These so-called “identical conditions” refer to the application of well planned and executed procedures to ensure identical conditions with tools that can be reasonably controlled. For instance, HAZ flaws can be introduced in the same target location, but the local micro-scale features can differ from one flaw location to another.
- There are no test standards for medium- and large-scale test specimens. Differences in test results may reflect differences in both material behavior and test procedures.

In summary, the determination of transferability from tests alone can be difficult without conducting a large number of tests, including large-scale tests. Given the time and cost associated with large-scale tests, this line of investigation is seldom pursued. Numerical analysis, in which various parameters can be varied systematically, is a valuable tool to determine the specimen transferability. Such analysis, complemented by selected experimental tests of different scales, is the most effective and practical approach to examining the transferability.

1.2 IMPACT

Material resistance to crack propagation is one of the key input parameters for the tensile-strain design of pipeline girth welds. Small-scale, CWP, and full-scale tests have been used for many years in the pipeline industry. These tests are being increasingly used in recent years for strain-based design of pipelines especially for the quantification of girth weld behavior under large longitudinal tensile strains. CWP tests have typically been used as quasi-structural specimens to evaluate the tensile strain capacity of pipeline girth welds [4,5].

The transferability of these test forms has not been thoroughly investigated. The lack of generally accepted test procedures for medium- and large-scale specimens further complicates the understanding and comparison of test data. It is therefore critical to address two interrelated

and critical issues: (1) consistent test procedures for medium- and large-scale specimens and (2) understanding the transferability of test specimens of different scales.

1.3 OBJECTIVE

The overall objectives of this work are as follows:

- (1) Develop a test methodology to measure the physical response of a finite-length surface-breaking flaw to axial loads applied to a girth welded linepipe section.
- (2) Determine the appropriate instrumentation to fully characterize the global stress/strain response of the CWP specimen during loading.
- (3) Evaluate the applicability of the test methodology for sub-ambient temperatures
- (4) Develop a standardized procedure for CWP testing that can be used over a wide range of variability in the test parameters.

1.4 SCOPE OF THIS REPORT

One of the primary goals of this work is to develop a consistent and standardized test procedure for conducting medium-scale tests on pipeline girth welds. In order to fully develop any test procedure, the range of applicability needs to be addressed. Physical test parameters such as specimen geometry, loading conditions and flaw geometry need to be clearly defined for test procedures or at the very least considered in the analysis. Environmental test parameters such as temperature and load/strain rates are also crucial to knowing the applicability of the test.

In Section 2, the CWP specimen used in this test program is detailed, followed by the specimen preparation process in Section 3. Section 4 describes the instrumentation used during this test program. The equipment required for this testing is specified in Section 5. The CWP test procedures employed in this project are introduced in Section 6, with detailed post-test analysis procedures given in Section 7. A summary and future work direction for the CWP testing is given in Section 8, with concluding remarks in Section 9.

This report does not include the development of a compliance function for the determination of flaw size or the development of J correlation equations; those topics are covered in subsequent topical reports [6]. Sample CWP test data is provided here in Section 7 only to describe the format of the data submitted to other collaborators.

1.5 TEST MATRIX

The entire test matrix consists of 34 test specimens and is shown in Table 1.

Table 1. CWP test matrix

Order of Test	Specimen ID	Flaw Location	Target Final Flaw Size (depth x width, mm x mm)	Clock Position (o'clock)	Test Temperature (°C)
1	BM-RT	BM (base metal)	3 x 50	N/A	Room Temp.
2	CWP-16	WMC (Weld Metal Centerline)	3 x 50	7:30	Room Temp.
3	CWP-03	HAZ (heat affected zone)	3 x 50	7:00	Room Temp.
4	CWP-01	WMC	6 x 30	1:30	Room Temp.
5	CWP-15	HAZ	6 x 30	6:00	Room Temp.
6	BM-LT	BM	3 x 50	N/A	-20
7	CWP-11	WMC	3 x 50	6:45	-20
8	CWP-19	WMC	3 x 50	5:30	-20
9	CWP-10	WMC	6 x 30	4:00	-20
10	CWP-12	HAZ	6 x 30	8:30	-20
11	CWP-02	HAZ	3 x 50	4:30	-20
12	CWP-23	HAZ	3 x 50	7:30	-20
13	CWP-20	WMC	3 x 50	2:15	Room Temp.
14	CWP-21	HAZ	3 x 50	4:00	Room Temp.
15	CWP-22	WMC	3 x 50	5:30	-20
16	CWP-14	WMC	3 x 50	5:15	-40
17	CWP-13	WMC	3 x 50	3:30	-40
18	CWP-18	HAZ	3 x 50	9:00	-40
19	CWP-17	HAZ	3 x 50	4:00	-40
20	CWP-05	HAZ	3 x 50	2:00	-20
21	CWP-07	WMC	2 x 75	8:00	-20
22	CWP-06	WMC	2 x 75	4:15	Room Temp.
23	CWP-08	HAZ	2 x 75	11:00	Room Temp.
24	CWP-09	HAZ	2 x 75	2:00	-20
25	CWP-24	WMC	6 x 30	2:00	Room Temp.
26	CWP-27	HAZ	6 x 30	2:00	-20
27	CWP-25	HAZ	6 x 30	4:30	Room Temp.
28	CWP-26	WMC	6 x 30	7:30	-20
29	CWP-28	WMC	3 x 50	9:30	-40
30	CWP-29	HAZ	3 x 50	11:00	-40
31	CWP-30	WMC	2.5 x 50	11:15	-20
32	CWP-31	HAZ	2.5 x 50	4:00	-20
33	CWP-32	HAZ	2.5 x 50	11:15	-20
34	CWP-33	WMC	2.5 x 50	4:00	-20

2 CURVED-WIDE-PLATE SPECIMEN

2.1 GENERAL CONSIDERATIONS

This section details the variables associated with the CWP specimens used in this study. Standardization of the CWP test is difficult due to the very wide variety of variables encountered for a test of this scale and complexity. The interaction between the variables and their applicable ranges affect the analysis of CWP test results. Therefore these variables, along with their boundary conditions, need to be explored, identified, analyzed and well documented for cross-comparability of CWP tests.

Inherent variations of base metal and weld-metal mechanical properties that include tensile and toughness properties are critical to the evaluation and application of CWP test results. Documentation of pertinent details must be provided for mechanical properties in addition to detailed accounts of the test procedure.

The following parameters must be well known and understood for CWP test results of girth welded linepipe to assess transferability of the test data based on scale and constraint:

- (1) specimen geometry and dimensions;
- (2) flaw geometry and dimensions;
- (3) flaw location;
- (4) mechanical properties of the flawed region;
- (5) stress-strain response of the remote material and flawed region material, such as;
 - strain-hardening characteristics,
 - uniform elongation, and
 - ductile-tearing characteristics;
- (6) mismatch of yield-to-tensile (Y/T) ratio and flow strength, and
- (7) weld design.

Test equipment, instrumentation and technical proficiency with mechanical testing, especially at this scale, is necessary to successfully perform CWP tests. Each specimen presents unique challenges as evidenced in this test program. Details to overcome these challenges with the use of consistent practices are detailed throughout this report.

2.2 MATERIAL

The linepipe steel used was specified as API-5L X100 material, with a 689 MPa (100 ksi) specified minimum yield strength (SMYS). Weld material information and processing parameters are subjects of several parts of the parent study [7]. Specific material properties are reported in other reports under this project [8]. It is important for cross-comparison of CWP data that the material properties are known.

2.3 SPECIMEN GEOMETRY

The CWP specimens tested in this program come from Focus Area 2 – Development of Optimized Welding Solutions for X100 Linepipe Steel. The specimens were removed from linepipe sections according to the specimen extraction plan found in Section 3.1. The specimens have a prismatic cross-section throughout the gauge section. They are dog-bone-shaped specimens with a straight-sided gauge section and parallel edges. There are two specimen

geometries used in the program; one with a thickness of 19.1 mm (0.75 in), designated as pipe A, and the other with a thickness of 14.3 mm (0.56 in), designated as pipe B. The outside diameters of the two pipes were also different: 914 mm (36 in) and 1067 mm (42 in), respectively.

2.3.1 Specimen Dimensions

A dimensioned schematic of the pipe A CWP specimen is shown in Figure 1. All dimensions remained the same for pipe B specimens except for the end-tab offset. The end-tab offset was changed to accommodate differences in specimen centroid. CWP testing was done with the assumption that the forces acting on the section mimic a purely longitudinal pipe stress. Hence, end-tab offset ensures that the machine load line coincides with the centroid of the specimen when the load is within elastic range to avoid bending loads. A detailed discussion of the end-tab welding is found in Section 3.7, and the specimen alignment is discussed in Section 6.1.

Table 2 summarizes the key specimen dimensions used for machining the CWP specimens in this study.

Table 2. Nominal dimensions of CWP test specimens

	Pipe A	Pipe B
Nominal Thickness	19.1 mm (0.75 in)	14.2 mm (0.56 in)
Gauge Width (chord)	254 mm (10 in)	254 mm (10 in)
Overall Length	1320.8 mm (52 in)	1320.8 mm (52 in)
Gauge Length	1016 mm (40 in)	1016 mm (40 in)
Overall Width	355.6 mm (14 in)	355.6 mm (14 in)
Fillet Radius	76.2 mm (3 in)	76.2 mm (3 in)

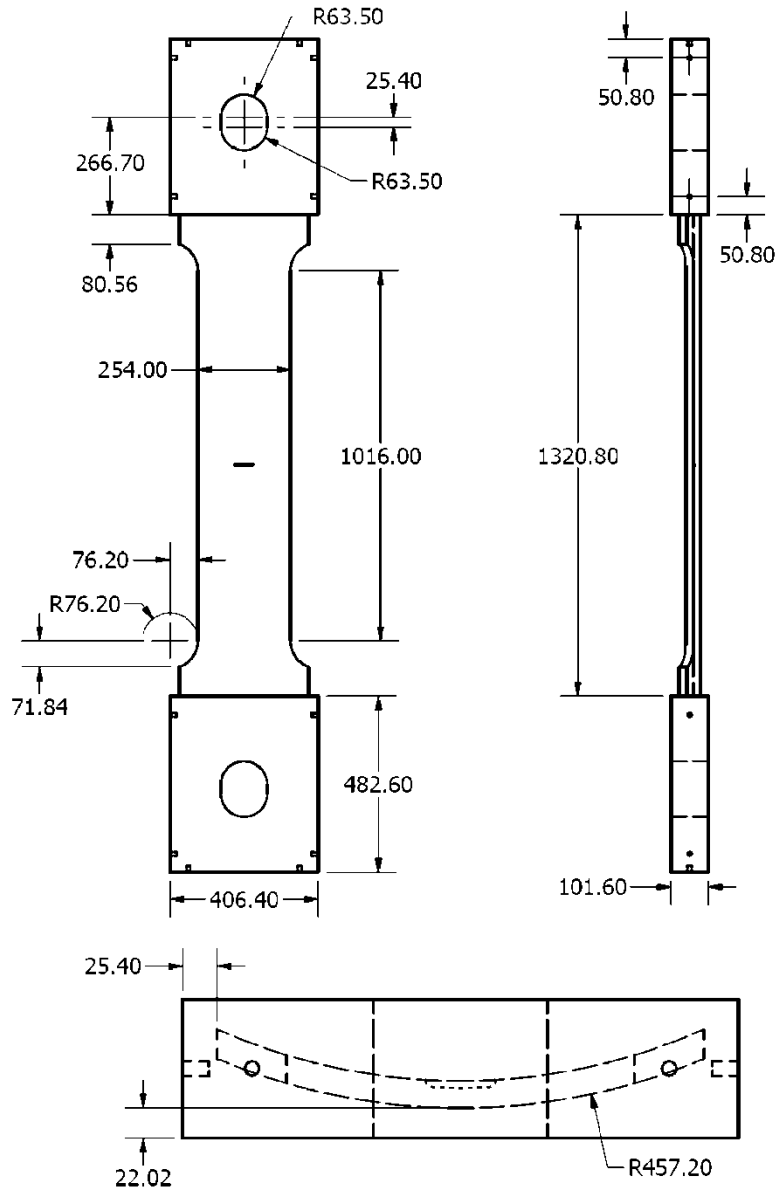


Figure 1. Dimensioned schematic of CWP specimen from 19.1 mm thick linepipe section, for pipe A.

(dimensions in mm)

2.3.2 Flaw Geometry

The surface-breaking flaw geometry used in this test program varied in shape slightly, depending on the method of notching, which is detailed in Section 3.5. Four notch geometries were specified in the test matrix. All flaws were introduced on the inside surface of the pipe. The prescribed flaw profile was an arc that matched the inside diameter dimension of the pipe to ensure that the depth remained constant along its entire length. Figure 2 illustrates a notch profile of a 3 mm x 50 mm flaw produced with an electric-discharge machining (EDM) process that was performed in two steps followed by fatigue pre-cracking. The details of notching and fatigue pre-cracking are covered in Sections 3.5 and 3.6, respectively. The sketch in Figure 2 demonstrates the profile of the flaw following the geometry of the pipe as opposed to being strictly semi-circular or semi-elliptical.

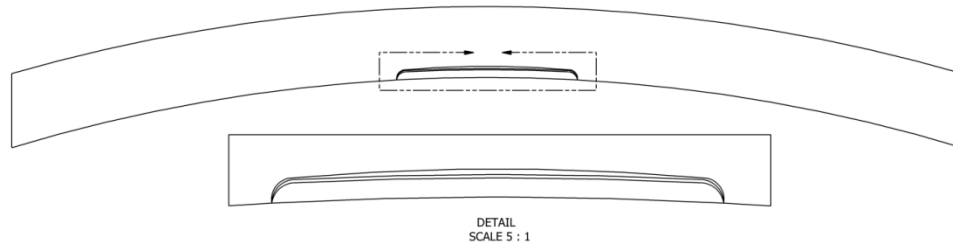


Figure 2. Placement and profile of the flaws introduced in the CWP specimen. This illustration is based on a 3 mm x 50 mm flaw. The lines in the figure represent the fatigue crack, the end of the second EDM step and the end the end of the first EDM step, from top to bottom, respectively.

The flaw geometries during this test program are provided in Table 3. The a/W ratio is the depth of the flaw divided by the nominal thickness of the pipe.

Flaws that were machined into the specimen with a slitting saw had the same central profile but much larger diameter ends as a result of the diameter of the slitting blade. The slitting saw method is described in detail in Section 3.5.

Table 3. Nominal surface-breaking flaw geometries of CWP test specimens

Notch Identifier	Target Depth - a (mm)	Surface Breaking Length - $2c$ (mm)	Nominal Thickness - W (mm)	a/W
2 × 75	2	75	19	0.11
2.5 × 50	2.5	50	14.2	0.18
3 × 50	3	50	19	0.16
6 × 30	6	30	19	0.32

2.3.3 Flaw Location

All flaws were oriented parallel to the girth weld and axially centered on the specimen to ensure symmetry, and as mentioned above, all flaws were introduced on the inside surface of the pipe section. The following location information pertains to the longitudinal location of the notches, referencing the weld geometry. Only two all-base metal specimens were tested. The remaining specimens contained girth welds at the midline of each specimen. The flaws introduced in the base metal specimens were located at the midline. The specimens designated as weld-notched specimens were notched along the circumferential centerline of the weld. The specimens designated as HAZ-notched specimens were notched so that the notch bisected the root weld cap and continued into the HAZ. The goal was to notch in such a way that fatigue pre-cracking finished with the crack tip in the HAZ. Figure 3 illustrates the location of the HAZ notches in a cross-sectional view of the weld. The alignment of the notches is critical to ensure that the majority of the flaw profile is within the material being tested.

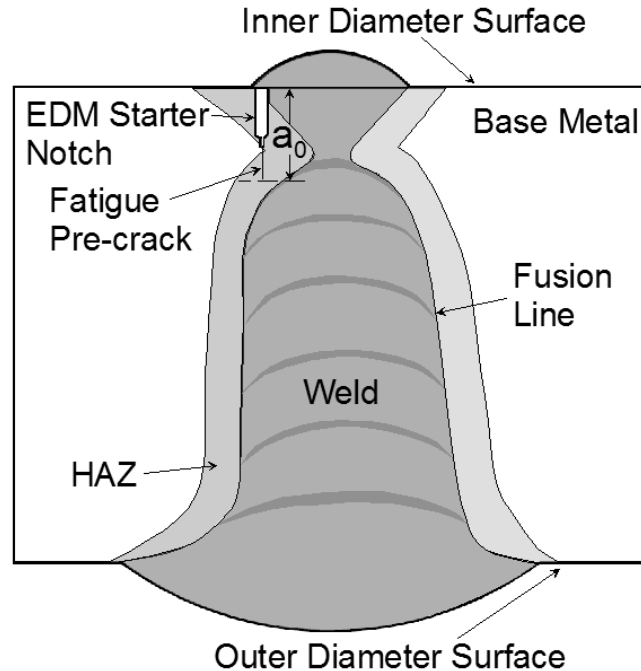


Figure 3. Specimens designated for HAZ testing were notched according to this schematic. The initial crack depth, a_0 , includes the depth of the EDM starter notch and the fatigue pre-crack depth.

3 SPECIMEN PREPARATION

3.1 SPECIMEN EXTRACTION PLAN

The specimen extraction plan for this program was developed at Lincoln Electric with guidance from CRES. The clock position of each specimen is provided in Table 1. The clock positions listed are for the axial centerline of each specimen. It is important for the cross-comparison of CWP data that the specimen extraction plans are known.

3.2 MACHINING

Pipe sections were received at Lincoln Electric, where axial strips were saw-cut from the pipe sections according to the specimen extraction plan. These blanks were then saw-cut to length, ensuring that the girth weld was located at the midline. The ends were beveled for welding to the end-tabs at first by hand grinding and subsequently by milling the ends to ensure a consistent bevel. The blanks were then milled to achieve the correct fillet and reduced-section profiles. Consistency between specimens was maintained with this process, and the edge finish was excellent compared to other methods of sectioning. Heat-producing cutting processes were not used to section or shape the specimens. The specimens tested were as close to the as-received/as-welded condition as possible.

3.3 SHIPPING CONSIDERATIONS

The program began with specimens that were already welded to end-tabs when they were received at NIST. The combined weight of each specimen exceeded 340 kg (750 lb). The shipping pallets constructed were not adequate for the first two shipments of specimens. Furthermore, these specimens were difficult to handle for test preparations, even with the proper crane and rigging equipment available at NIST. The first two specimens received at NIST are

shown in Figure 4. Although extra shipping steps and added expenses were incurred, a decision was made for subsequent specimens to complete most of the specimen preparation and pre-cracking prior to welding the end-tabs. Each specimen section weighed approximately 34 kg (75 lb). Specimens without end-tabs were shipped in specially-constructed shipping crates capable of withstanding the weight and rigorous handling of truck freight-shipping methods. Once the specimens were prepared and pre-cracked, they were shipped back to Lincoln Electric together with the end-tabs from the most recent test for welding. Figure 5 shows a photograph of the shipping crate designed and fabricated at Lincoln Electric for shipping specimens and end-tabs. Two shipping crates were manufactured to accommodate the test schedule. A schedule was maintained so that NIST was supplied a flow of test specimens while Lincoln was resupplied with end-tabs and newly prepared specimens for welding.



Figure 4. First shipment of specimens received at NIST. The first two specimens were base metal specimens without girth welds.



Figure 5. Shipping crate designed and fabricated at Lincoln Electric for shipping CWP specimens between NIST and Lincoln Electric.

3.4 SURFACE PREPARATIONS

When received at NIST, each pipe section was covered in mill-scale and corrosion. In order to apply the instrumentation prescribed in Section 4.1, the surface had to be cleaned ensuring proper bonding of the instruments to the surface of the specimen. Wire wheels and abrasive disks were used to remove the scale and corrosion. Removal of the scale and corrosion was performed in a way to minimize material reduction. Some specimens had severe pitting in the areas designated for instrumentation installation. Only the areas necessary for installation were prepared, with care taken to avoid gouges and undercutting near the weld caps. Figure 6 is a photo of the inside-diameter surface of a specimen instrumented with strain gages and linear variable differential transformers (LVDTs), the details of which will be elucidated in Section 4. The notable details in this photo are the relatively small areas prepared for gaging.



Figure 6. Photograph of the ID surface of a specimen, showing the minimal surface changes necessary to prepare the surface for instrumentation. Strain gages and LVDTs are installed on the specimen in this photo. This was a room-temperature test, so thermocouples are absent; however, the area necessary to install thermocouples was very small.

3.5 NOTCHING

Two different procedures were used to introduce a notch in the CWP specimen. A purpose-built slotting saw designed and fabricated for notching specimens was replaced by a sinker electric-discharge machining (EDM) technique. The saw-cutting method was used to introduce notches in which the notch was the final flaw. The EDM technique was used to introduce starter notches for specimens where the final flaw size would be achieved through fatigue pre-cracking. The

saw-cutting method was only used on specimen CWP-03, specimen CWP-16 and the base metal specimen tested at room temperature (BM-RT). The saw-cutting method is reported in the next section, but was replaced by the EDM method to optimize available resources and improve accuracy.

3.5.1 Saw-Cut Notches

A surface notching method was developed to introduce a notch into the inside diameter (ID) surface of the pipe with an electric motor-driven slitting saw blade. The blades had a thickness of 0.5 mm (0.020 in) and a diameter of 70 mm with 72 teeth. Two different blades were used: one with a square tooth, and another with a 60° included-angle tooth for the final 0.5 mm of notch machining. Figure 7 is a photograph of the slitting saw head.



Figure 7. Photograph of the slitting saw head close to the ID surface of the base metal specimen

Welded specimens were prepared for the saw-cutting method first by grinding the weld toe flush with the ID surface of the upper plate. The CWP specimen was then loaded into the saw, in a position such that the centerline of the CWP specimen coincided with the centerline of the saw. A beveled edge slitting saw blade was installed, and the process was repeated to finish with a cut depth of 3 mm.

3.5.2 EDM Notches

A sinker EDM machine was used to introduce a notch where the notch shape was controlled by use of a profiled copper-tungsten electrode. The copper-tungsten electrodes were cut and profiled from a flat plate with a wire EDM machine. Two values of electrode thickness were selected for machining the notch: 0.05 mm thick and 0.41 mm thick. In order to prepare the weld region on the ID surface, the toe of the weld was removed with the EDM, with an electrode that matched the contour of the ID surface of the plate. This electrode was approximately 25 mm thick and spanned the surface arc length, matching the surface breaking length of each notch as

described in Table 3. The weld toe was machined away until it was flush with the upper plate (inner diameter surface) of the weld, as described in Figure 8.

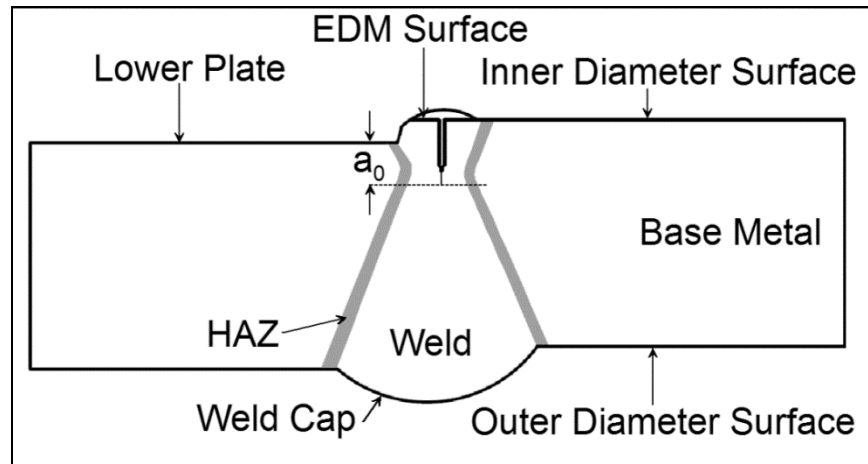


Figure 8. An exaggerated illustration showing the plate misalignment, the EDM reference surface and a notch placed in the weld. This diagram also illustrates the datum for initial crack depth, a_0 , measurement.

The EDM notching process was completed in two stages. The depth value of each EDM notch was referenced to the surface of the lower plate of the weld. First, the thick electrode was used to cut to the final depth, minus 0.35 mm, which left a notch thickness or gap of 0.50 mm due to over burn. The thin electrode was used to remove an additional 0.35 mm to obtain the final notch depth.

Because no accepted CWP standards exist, ASTM standards for fracture mechanics testing were used as guidelines in selecting the geometries of the various notches. ASTM E1820 requires that the tip of a V-shaped notch has a root radius of less than 0.08 mm (0.003 in). The thin electrode (0.05 mm) provided a starter notch with a root radius of approximately 0.075 mm. The 0.41 mm thick electrode was selected to provide a final notch thickness of 0.50 mm. This matched the thickness of the notch introduced with the slitting saw method, which also allowed the placement of crack mouth opening displacement gages without use of knife edges.

A schematic diagram showing the side profile of the EDM notch is shown in Figure 9. For illustration, a flaw 3 mm deep is shown. The detailed electrode dimensions and depth of notching for each of the four notch geometries is given in Table 4.

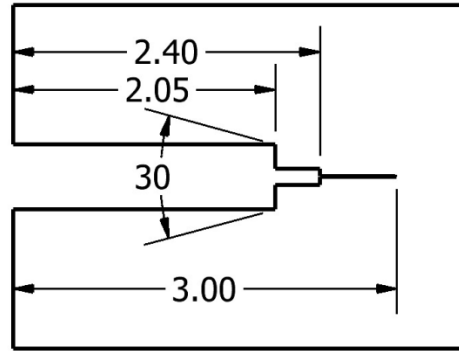


Figure 9. Cross-section diagram describing the notch depths and relative geometry of the EDM starter notch with respect to the final flaw depth for the 3 mm x 50 mm flaw. All depths given in mm with the included angle in degrees.

Table 4. Nominal notch geometries for 0.6 mm pre-crack requirements

Notch Identifier	Target Depth, a (mm)	Thick Electrode Depth (mm)	Final Electrode Depth (mm)
2 x 75	2	1.05	1.40
2.5 x 50	2.5	1.55	1.90
3 x 50	3	2.05	2.40
6 x 30	6	5.05	5.40

3.6 FATIGUE PRE-CRACKING

Five specimens: BM-RT, CWP-01, CWP-03, CWP-15 and CWP-16, were not pre-cracked. BM-RT is the base metal specimen that contained a 3 mm x 50 mm saw-cut notch, and were tested at room temperature. CWP-03 and CWP-16 are both 3 mm x 50 mm saw-cut notches in the HAZ and weld, respectively, and were tested at room temperature. CWP-01 and CWP-15 both contain 6 mm x 30 mm EDM notches in the weld and HAZ, respectively, and were also tested at room temperature. With the exception of these five specimens, all other specimens were notched to the depths described in Table 4, followed by pre-cracking.

Because fatigue pre-cracking is time intensive, a second test machine was set up and dedicated to fatigue pre-cracking. This allowed specimen preparation and specimen testing to be conducted in parallel. The dedicated machine selected for fatigue pre-cracking had insufficient physical capacity to fatigue pre-crack in tension. A four-point bending method was developed at NIST to extend the notches to the prescribed flaw geometry [6]. The development process was extensive, and several iterations were completed to accommodate many variables necessary to develop a predictive capability and to justify the highest confidence in flaw geometry prior to testing the CWP specimen.

The loading arrangement used is shown in Figure 10. The outer span loading supports consisted of contoured convex surfaces with a major radius of 432 mm, a minor radius of 100 mm, and an outer span spacing of 178 mm. The inner-span loading configuration consisted of two adjacent straight rollers of 32 mm diameter, resulting in an inner span of 32 mm. The inner and outer

spans were chosen based on finite-element modeling to optimize the stress intensity factor at the notch without yielding the outer fiber of the specimen.

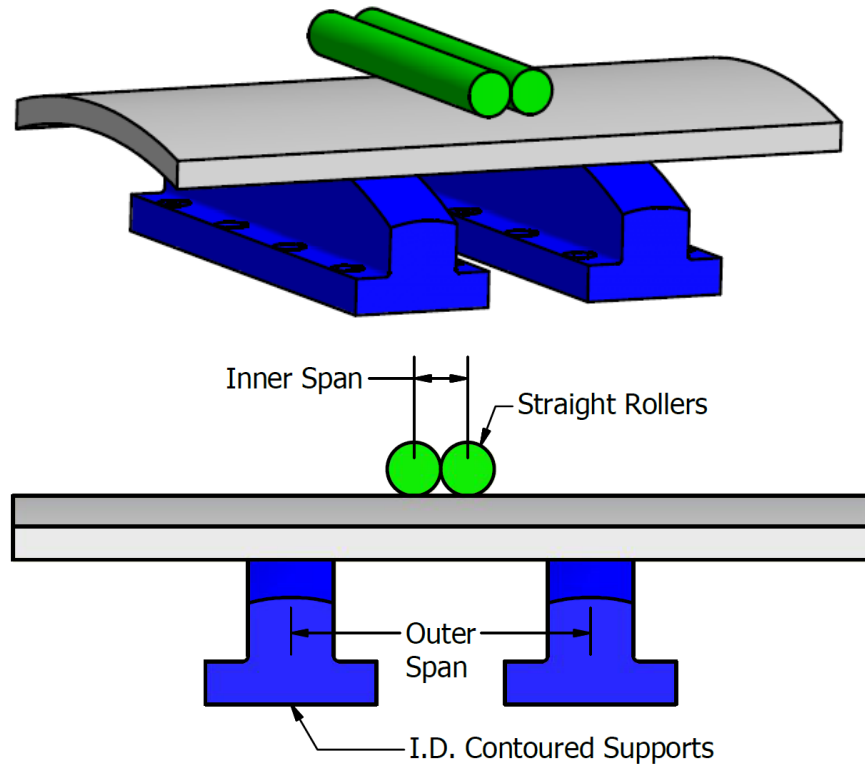


Figure 10. Schematic of contoured outer-span loading supports (blue) and straight-roller inner-span (green) loading arrangement used in four-point bending fatigue pre-cracking of curved-wide-plates [6].

Following the introduction of the EDM starter notch, the specimens were prepared for fatigue pre-cracking. Various scribe lines were introduced to the specimen for alignment purposes. A centerline longitudinal to the pipe axis was scribed along the ID and OD surfaces to align the crack extension gauge and align the inner-span loading fixture on the OD of the specimen.

The initial crack depth was measured by marking the end of a piece of feeler gauge or shim stock that had a thickness of 0.05 mm (0.002 in) and a rounded end with a black permanent marker. The feeler gauge was inserted into the EDM starter notch and moved until it slipped down to the bottom of the thinnest portion of the EDM starter notch. A thicker feeler gauge (0.2 mm thick) was inserted behind the thin feeler gauge to prevent bending or shifting. Then a fresh scalpel blade was scraped across the surface of the weld toe that had been removed by the first EDM process to scribe a surface indication line on the black surface of the feeler gauge. The feeler gauge was removed, and the distance between the scribe line and the tip of the rounded surface was measured. The measurement method consisted of placing the rounded tip of the shim stock against the anvil of a digital caliper and adjusting the caliper spacing until the opposing anvil was aligned with the scribe line. Calipers were then used to measure the height differential between the EDM surface, to which the crack depth measurement was referenced, and the ID surface of

the lower plate. The difference between the two measurements was taken as the EDM starter notch depth, a_0 , which is depicted in Figure 8.

The fatigue crack growth rate was targeted at one microinch ($1 \mu\text{in} = 0.0254 \mu\text{m}$) per cycle. This was varied slightly between specimens to complete the fatigue pre-cracking procedure in approximately 2×10^4 cycles. The loading ratio R is the ratio between the minimum stress intensity factor K_{min} , and the maximum stress intensity factor K_{max} . The loading ratio was maintained at 0.4 for all specimens.

A ring-type clip gauge was installed into the EDM starter notch and remained in place by spring force against the internal notch faces. This clip gauge was used to measure the crack mouth opening displacement (CMOD). The outer span, contoured loading supports were coated with a layer of high-pressure bearing-grease, and the plate was then loaded into a servohydraulic mechanical test frame of 1 MN capacity and placed ID side down upon the contoured loading supports. The specimen was positioned such that the edge marks were aligned with the reference edges of the contoured loading supports and centered laterally on the contoured loading supports. The inner-span loading fixture was then placed on the OD surface of the specimen and aligned with the centerline of the specimen and the horizontal line that was offset from the notch centerline by 32 mm to position the inner-span loading fixture symmetrically about the starter notch. The servohydraulic actuator was then lowered into position, and a preload of approximately 4.5 kN was applied. A program was initiated to apply 10^4 cycles at 12 Hz with 4.5 kN to 45 kN force to seat the specimen. Seating was followed by 100 cycles at 1 Hz with load levels corresponding to K_{min} and K_{max} . The program then measured five loading and unloading cycles at 1 Hz from force levels corresponding to K_{min} and K_{max} while recording force and CMOD data. These data were evaluated, and the stiffness and compliance data were recorded and averaged as the compliance at zero cycles; the assumption is that no crack propagation occurs in the first 10^4 cycles. A second program was then executed that loaded the specimen between K_{min} and K_{max} at 12 Hz in 10^3 cycle intervals, followed by a slow (1 Hz) compliance measurement. These compliance data were evaluated and recorded. The instantaneous crack depth a_i was calculated at each 10^3 cycle interval. A plot of compliance versus cycles was developed for each specimen, and the intercept compliance value C_0 was determined by the shape of the data. When the data for compliance versus cycles became linearly related, the portion of the data that was linear was selected, and a linear regression fit was determined where the intercept value of the linear regression fit corresponded to the zero-cycle point. The intercept of the regression line on the compliance axis established the value C_0 . Some specimens exhibited a delay in crack initiation, evidenced by compliance data that were insensitive to loading cycles. In this case, the cycle count data were offset by the number of cycles required to achieve a deviation from the initial non-linear behavior to ensure that the intercept compliance value was not artificially low due to delayed initiation of the fatigue crack. The results of this method are shown in Figure 11 and Figure 12.

It has been shown previously with finite element modeling (FEM) [9] that the stress intensity factor K for the four-point bending loading configuration shown in Figure 10 can be approximated by bending in a flat plate. Closed-form solutions for the stress intensity factor for a surface crack in a flat plate under pure bending were determined based upon ASTM E740-03 annex A2, from equations originally derived by Newman and Raju [10]. For bending with a nominal outer fiber stress σ_b , at the deepest point on the crack periphery,

$$K = \sigma_b \sqrt{\pi a} \left(\frac{M}{\Phi} \right) H, \quad (1)$$

where

$$M = \left\{ 1.13 - 0.09 \left(\frac{a}{c} \right) \right\} + \left\{ -0.54 + \left(\frac{0.89}{0.2 + \left(\frac{a}{c} \right)} \right) \right\} \left(\frac{a}{B} \right)^2 + \left\{ 0.5 - \frac{1}{0.65 + \left(\frac{a}{c} \right)} + 14 \left(1 - \left(\frac{a}{c} \right)^{24} \right) \right\} \left(\frac{a}{B} \right)^4, \quad (2)$$

$$H = 1 - \left\{ 1.22 + 0.12 \left(\frac{a}{c} \right) \right\} \left(\frac{a}{B} \right) + \left\{ 0.55 - 1.05 \left(\frac{a}{c} \right)^{0.75} + 0.47 \left(\frac{a}{c} \right)^{1.5} \right\} \left(\frac{a}{B} \right)^2, \text{ and} \quad (3)$$

$$\Phi^2 = 1 + 1.464 \left(\frac{a}{c} \right)^{1.65}. \quad (4)$$

Here, a is the crack depth, c is the crack half-width and B is the plate thickness. For the curved-wide-plates, the relationship between the applied force and outer fiber stress can be determined in two ways. First, stress can be measured by instrumenting an un-notched test section with a strain gage at the location of the notch. Second, through mechanics, the stress within a member in bending can be determined with

$$\sigma = \frac{My}{I_x}, \quad (5)$$

where M is the moment about the neutral axis, y is the perpendicular distance from the neutral plane to the point of interest and I_x is the second moment of inertia about the neutral x-axis. The moment M for four point bending can be determined from

$$M = \frac{P}{4} (l_1 - l_2), \quad (6)$$

where l_1 and l_2 are the outer and inner loading spans, respectively, and P is the applied force. The relationship between force and stress intensity for fatigue pre-cracking was determined using Equation (1) for each fatigue pre-crack geometry listed in Table 4, and is listed in Table 5. Also listed in Table 5 is the typical stress intensity factor amplitude ΔK used for each notch geometry during fatigue pre-cracking.

Table 5. Stress intensity factor and typical fatigue pre-crack stress intensity factor amplitude levels

Final Notch Geometry $a \times 2c$ (mm \times mm)	Starter Notch Geometry $a \times 2c$ (mm \times mm)	K (ksi \sqrt in)	K (MPa \sqrt m)	Typical Fatigue Pre-Crack ΔK (MPa \sqrt m)
2 \times 75	1.4 \times 73.3	0.5586	0.1380	11.44
2.5 \times 50	1.9 \times 48.3	1.1908	0.2942	17.31
3 \times 50	2.4 \times 48.3	0.6826	0.1686	15.58
6 \times 30	5.4 \times 28.3	0.7080	0.1749	16.22

A means of accurately predicting fatigue pre-crack depth based upon compliance data during loading from applied force versus crack mouth opening displacement (CMOD) data has been developed and reported [9]. The relationship between compliance and crack depth is shown in Figure 11. Figure 11 shows the offset compliance versus optically measured crack depth for the various notch geometries used in base metal. Base metal segments of tested specimens were notched and fatigue-cracked with the loading configuration shown in Figure 10. Compliance data were gathered periodically. Following a compliance measurement, a fatigue marker band was introduced to place an artifact on the fracture surface by which post-test optical measurements could be made to correlate actual crack depth to compliance data. Figure 13 shows an example of a fracture surface showing marker bands from a liberated crack [6]. The fatigue marker bands were introduced by reducing the stress intensity factor amplitude to approximately 60 % of that during regular fatigue crack growth for between 5×10^4 and 15×10^4 cycles.

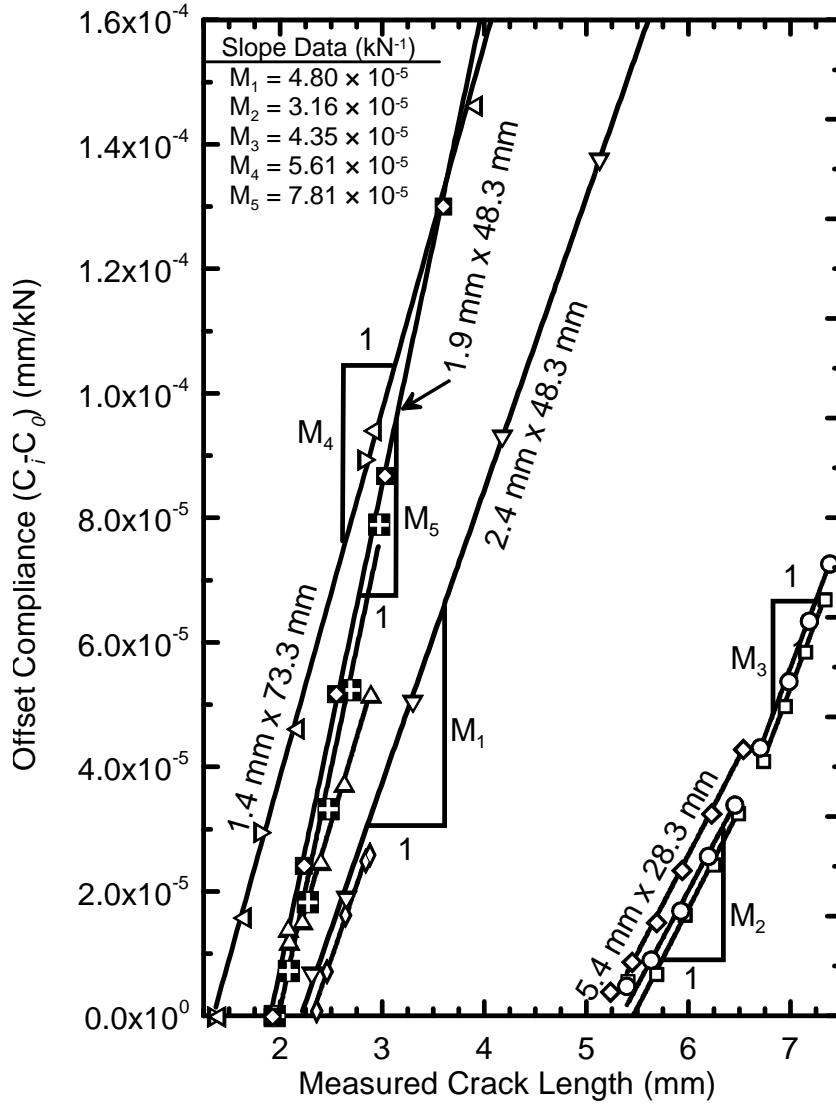


Figure 11. Offset compliance versus optically measured crack depth data for CWP notch geometries in base metal.

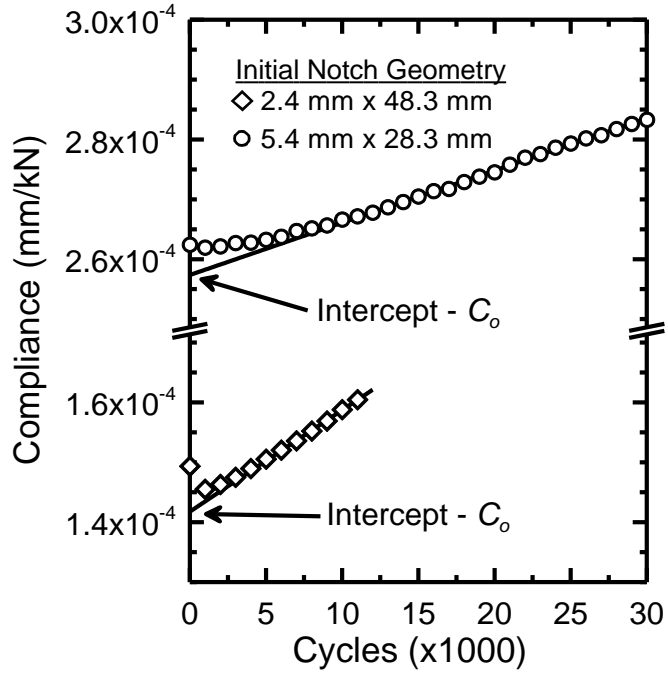


Figure 12. Compliance versus the number of cycles plot for two starter notch geometries.

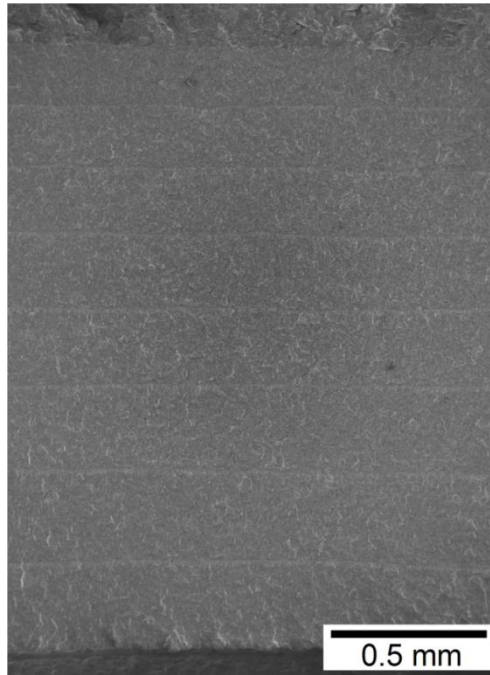


Figure 13. SEM image of fatigue pre-crack fracture surface showing fatigue marker bands. Initial EDM notch geometry was 5.4 mm deep by 28.3 mm wide [6].

Figure 12 shows the measured compliance versus the number of loading cycles for two initial starter notch geometries, 2.4 mm x 48.3 mm, and 5.4 mm x 28.3 mm. As seen in Figure 12, for both starter notch geometries, the initial response to cyclic loading is nonlinear, but after a certain number of loading cycles the compliance-versus-the number of cycles relationship becomes linear. Analysis of the fracture surfaces indicated that the nonlinear portion of the curve resulted from different crack initiation rates between the deepest point in the EDM notch and the surface of the EDM notch, which was attributed to the difference in the notch root radii around the EDM notch periphery. The ordinate intercept of the linear portion of the compliance-versus-the number of cycles data in Figure 12 was termed the compliance intercept C_0 . The compliance data in Figure 11 were offset by C_0 to correct for minor specimen-to-specimen differences such as misalignment of the specimen in the loading fixtures and eccentric pipe sections about the girth weld. Eccentricity of the girth welded pipe sections result in small torsion moments about the centerline of the specimen and consequently asymmetry in the stress intensity factor along the flaw periphery.

Figure 11 shows that a linear relationship exists between the offset compliance data and the crack depth, in which the measured compliance data are offset by the intercept compliance value C_0 from Figure 12. With the slope values listed in table 3-3, for each starter notch geometry in Figure 11, a predictive formula was developed to accurately predict instantaneous crack depths during the fatigue pre-cracking procedure. For an instantaneous crack depth, the linear relationship between the instantaneous compliance C_i characteristic slope M , and instantaneous crack depth a_i , is given by

$$C_i = Ma_i + R, \quad (7)$$

where R is an arbitrary intercept. When the initial conditions are known for the fatigue pre-crack plate, such as the initial crack depth a_0 and the initial compliance C_0 the instantaneous crack depth can be determined by

$$a_i = \frac{C_i - C_0}{M} + a_0. \quad (9)$$

Table 6. Offset Compliance versus Crack Depth Correlation Slope Values

Final Notch Geometry $a \times 2c$ (mm \times mm)	Starter Notch Geometry $a \times 2c$ (mm \times mm)	Slope of Offset Compliance versus Crack Depth M (kN^{-1})
2×75	1.4×73.3	5.61×10^{-5}
2.5×50	1.9×48.3	7.81×10^{-5}
3×50	2.4×48.3	4.80×10^{-5}
6×30	5.4×28.3	3.16×10^{-5}

Once the intercept compliance value was obtained, the spreadsheet was updated with the value and the predicted crack depth data were calculated from instantaneous compliance data at 10^3 cycle intervals. When the target crack depth was achieved, the pre-cracking procedure was arrested and the specimen was unloaded and removed.

3.7 WELDING END-TABS

Once surface preparation and pre-cracking were completed, the specimens were shipped back to Lincoln Electric to have the end-tabs welded on. A welding jig was manufactured at Lincoln Electric to consistently set up and weld the end-tabs to the specimens. It consisted of a thick steel plate with a tubular frame to prevent misalignment. The plate had access slots cut to provide access to both sides of the specimen while maintaining the same set up. End-tabs were welded to the plate to prevent movement, the specimen was placed between the end-tabs, aligned, supported and tack welded to the end-tabs.

Two different pipe section geometries required different grip offsets. The centroid positions of the test gauge section determined the grip offset and alignment of the specimens for welding, and are shown in Figure 14.

The end-tabs were machined from HSLA-100 plates. The design of the specimen and the weld parameters were determined to eliminate the possibility of grip failure during the test.

Table 7 contains the weld parameters for this process. Preheating was performed in a large oven that accommodated the entire specimen assembly.

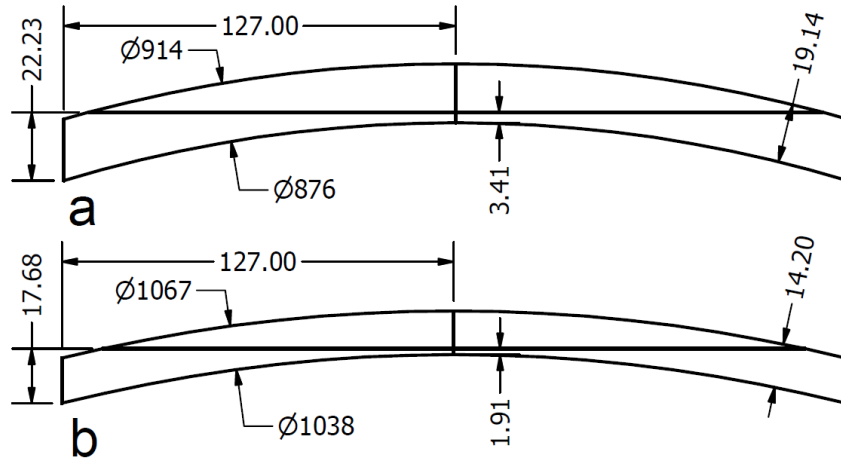


Figure 14. Centroid positions of the gauge section of the CWP specimen of the two pipe geometries (top) pipe A (19.1 mm thick) and (bottom) pipe B (14.20 mm thick). Units given in mm.

Table 7. End-tab welding process parameters

Method	Gas Metal Arc Welding (GMAW)
Root Gap	1.6 mm - 2.3 mm (1/16 in – 3/32 in)
Wire	AWS ER100S-G
Wire Diameter	1.1 mm (0.045 in)
Shielding Gas	90:10 Ar:CO ₂
Current Mode	DC+
Pulse	Semi-Automatic
Wire Feed Speed	9.5 m/min - 10 m/min (375 in/min - 400 in/min)
Voltage	28 V – 29 V
Travel Speed	230 mm/min - 255 mm/min (9 in/min - 10 in/min)
CTWD	16 mm – 19 mm (5/8 in – 3/4 in)
Pre-Heat	100 °C -125 °C (212 °F – 257 °F)
Sequence	Pass 1 – OD side of specimens Pass 2-4 – ID side of specimens Pass 5&6 – OD side of specimen

4 INSTRUMENTATION

4.1 INSTRUMENTATION PLAN

One of the overall objectives of this project is to understand the fracture resistance to flaw growth of the X100 welds. The fracture resistance is often represented by resistance curves, which are typically given as a function of the fracture toughness (J integral or CTOD) versus flaw growth. In order to satisfy the needs of this fracture mechanics-related study, many factors about the specimen and the test must be known. During the test it is important to have an understanding of the remote strain behavior of the specimen away from the flaw. The constraint conditions and the transferability of the test data rely heavily on the knowledge of the remote pipe response to axial loading.

This section of the report details an extensive array of instrumentation that was employed to determine the remote-strain behavior and the flaw growth behavior of the specimens. Photoelastic film was used on several room-temperature tests to visually capture the remote-strain behavior. To quantify this behavior, strain gages were installed to measure local strain at certain remote locations. The strain gages used had a gauge length of 0.25 in (6.35 mm); these gages were used in conjunction with LVDTs. The LVDTs were installed over much larger gauge lengths to determine the average remote strain and to also evaluate the amount of bending that occurred in the specimen as a result of the test configuration. A clip gauge to measure CMOD is used to determine the amount of flaw growth, to detect tearing, and to characterize crack tip blunting during the test. When applicable, temperatures during the test were measured with thermocouples that were welded to the specimen surface. Each of the sensors had unique calibration requirements that are detailed in this section. Finally, the data acquisition system is discussed in this section. The instrumentation layout schematic shown in Figure 15 indicates the location of 15 strain gage “T” rosette pairs (30 gages total), 6 LVDTs and their associated end points, thermocouples, photoelastic coating, and a CMOD clip gauge.

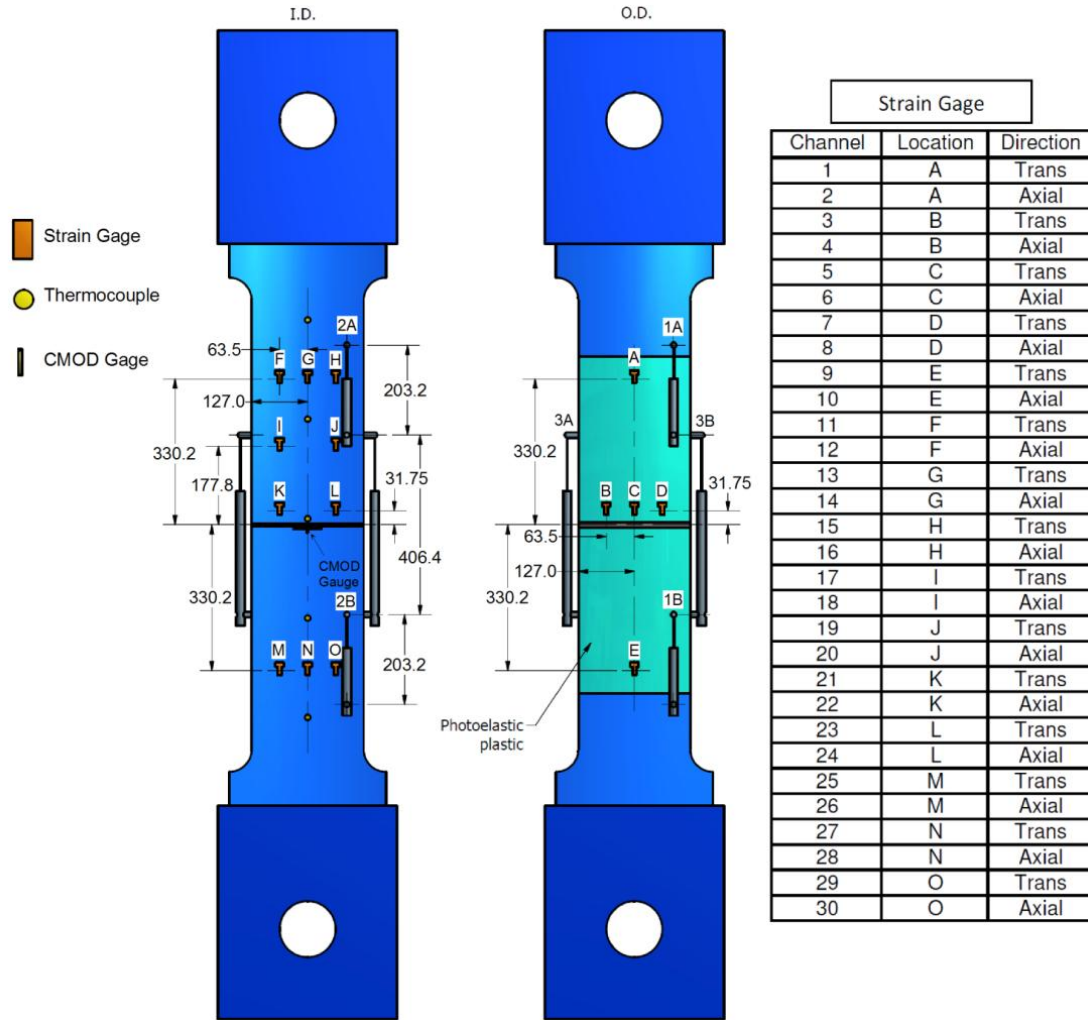


Figure 15. Schematic diagram of the instrumentation layout for the CWP testing. Dimensions are given in mm.

4.2 PHOTO-ELASTIC FILM

Photoelastic methods can be used to determine stress distribution in a material or on a component. The method is frequently used to verify analytical models and determine areas of high stress intensity, identifying locations that need additional attention or quantification. The method employed here used a transparent birefringent plastic sheet adhered to the outside diameter surface of the specimen. A specimen installed in the test frame is shown in Figure 16. In this photograph, the photoelastic film can be seen along with the polarizing sheet installed over the specimen. Photographs and video of the specimen response during testing were taken on several room-temperature tests.



Figure 16. Outside diameter side of the specimen showing the installation of the photoelastic film covered by the polarizing sheets on the specimen. Cut-outs in the photoelastic and polarizing film allowed the installation of the LVDTs and strain gages.

4.3 STRAIN GAGES

Uniaxial strain gages were installed in each of the locations prescribed in Figure 15. The gages were 350 Ω gages with a gauge length of 0.25 in (6.35 mm). They were installed in a “T” pattern, creating a biaxial rosette at each installation location. The strain gages were used to quantify the strain response at various points on the specimen. Strain gages were conditioned and amplified to provide a high-level analog signal to the data acquisition system. The manufacturer’s recommended installation procedure that met the guidelines established in ASTM E1237 [11], was followed.

4.4 LINEAR VARIABLE DIFFERENTIAL TRANSFORMERS

The remote strain response of CWP specimens is typically measured with LVDTs. The LVDTs were attached to the specimen on two 0.25-in studs that were welded onto the specimen surface with a capacitive discharge stud welder. LVDTs were powered, conditioned and amplified to provide a high-level analog signal to the data acquisition system. Photos showing the installation of the LVDTs can be seen in Figure 6 and Figure 16.

4.5 CRACK MOUTH OPENING DISPLACEMENT (CMOD) GAUGES

The CMOD gauges were a ring-type clip gauge with teeth that fit inside the notch. The teeth of the gauge were 0.025 in (0.6 mm) long, providing enough spring force to remain in the notch. A schematic of the clip gauge teeth engagement is found in Figure 17. After several instances in which the gages popped out of the notch during the test, a spring mechanism was devised to hold the gauge in the notch. Initially, three CMOD gauges were used to determine the symmetry of the test. The flaw opened with symmetry, so only one centrally installed CMOD gauge was used on subsequent tests. Figure 18 is a photograph of the CMOD gauge installation.

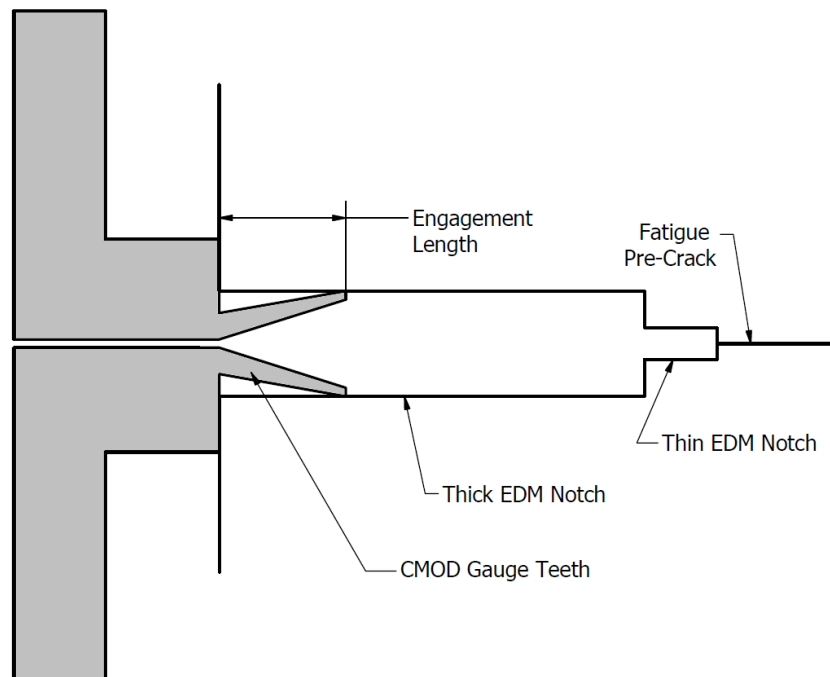


Figure 17. Schematic of the engagement of the clip gauge teeth in the notch of the specimen.



Figure 18. Inside-diameter side of the specimen, showing the installation of the CMOD gauges in the notch.

4.6 THERMOCOUPLES

When required, thermocouples were welded to the surface of the specimen. Two thermocouple patterns were used throughout the test program. Both patterns used ten thermocouples, five each on the OD and ID surfaces of the specimen. The first pattern consisted of a linear pattern of equally spaced thermocouples across the diagonal of the specimen on each surface. Due to the location of the notch, the center thermocouple was placed 50 mm above the mid-gauge length on the OD surface and 50 mm below the mid-gauge length on the ID surface. This pattern formed an “X” pattern between the OD and ID thermocouples. This pattern was determined to be unnecessary due to the uniformity of the environmental chamber. On subsequent samples, all thermocouples were placed along the longitudinal centerline of the specimen. The mid-gauge thermocouples were placed 50 mm above and below the mid-gauge length for the OD and ID surfaces, respectively, and the remaining thermocouples were positioned at 250 mm and 500 mm above and below the mid-gauge length.

4.7 CALIBRATIONS

All instrumentation calibrations were performed according to ASTM standards for the respective sensor types. Since quantification was not necessary, the response of the photoelastic film to strain was not calibrated.

Strain gages are not calibrated as individual sensors; however, the conditioners were calibrated at the factory, and the manufacturer provided gage-factor data to accurately set up the conditioners. The installation of the strain gages was verified in accordance with the manufacturer’s recommendations. The conditioner signal outputs were calibrated with the data acquisition system with a shunt calibration technique. The LVDTs were calibrated end to end (sensor to

data display) with a digital displacement calibrator. End to end calibrations were also performed on the CMOD gauges with a calibrated micrometer head according to ASTM E83 [12].

Thermocouples were made from a spool of thermocouple wire calibrated at the manufacturer. The thermocouple data acquisition system was verified with a handheld thermocouple simulator according the practices defined in ASTM E2730 [13].

The test equipment described in section 5 was calibrated by the manufacturer on-site at NIST. The manufacturer maintains certification to conduct calibrations by the American Association for Laboratory Accreditation (A2LA). The manufacturer certified the accuracy of both the force transducer and the displacement transducer. A calibration block was manufactured from HSLA-100 plate steel to carry the full load of the frame capacity. Figure 19 is an annotated photo of the calibration set up.

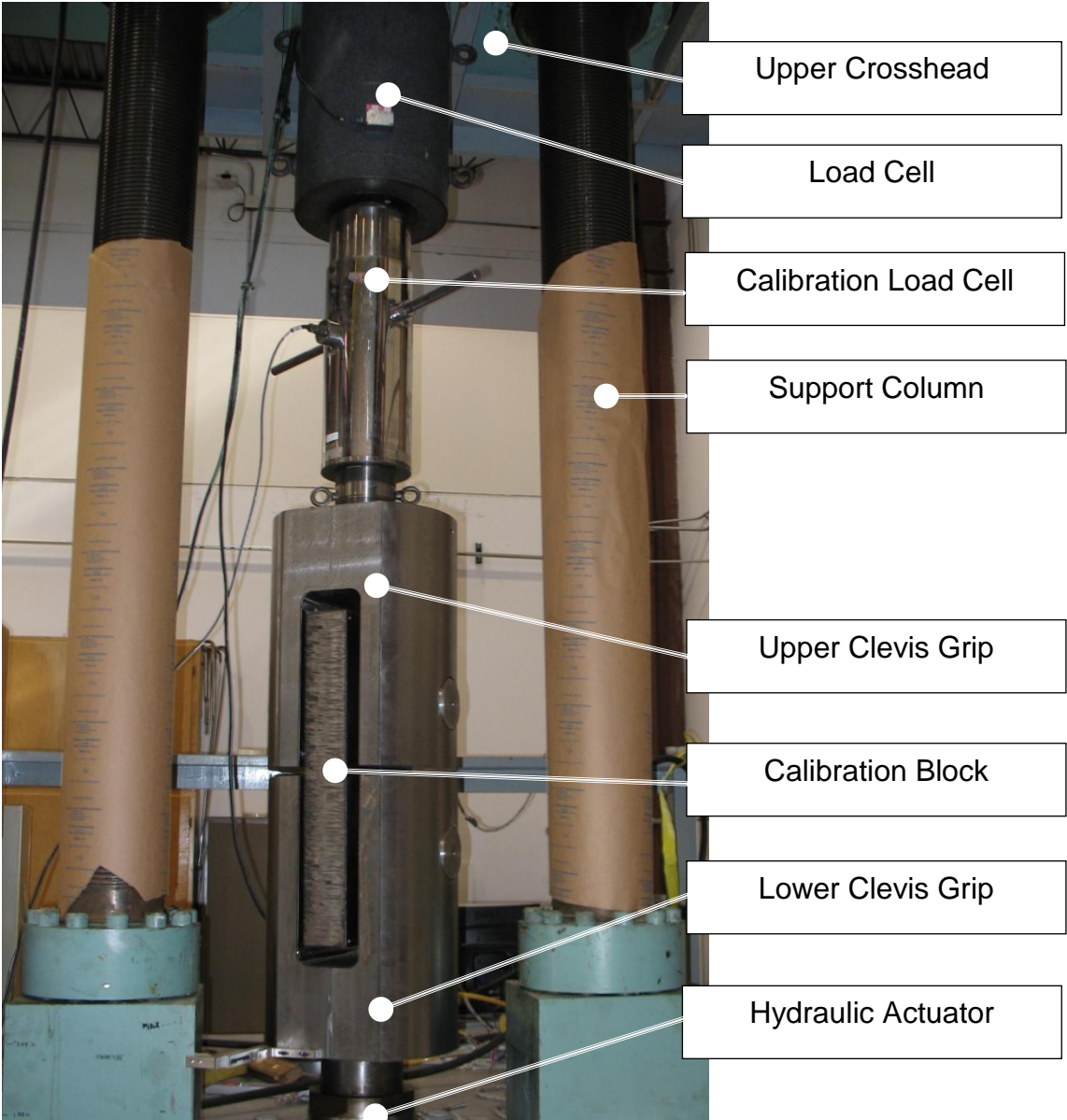


Figure 19. Test frame showing the specimen loading configuration. The location of the upper crosshead, testing load cell, calibration load cell (not present during normal testing), frame support columns, clevis grips, the calibration block and the hydraulic actuator are indicated.

4.8 DATA ACQUISITION

Two data acquisition systems were employed in this program to ensure redundancy to prevent data loss. The primary data acquisition systems were commercially available systems that were integrated into purpose-written software for this test program. Three different signal-conditioning systems were used, one for LVDT input signals, a second for strain gage input signals and the last for temperature with calibrated electronic cold junctions.

The LVDTs were connected to the LVDT conditioner and a high-level (± 10 V) signal was produced that was proportional to the sensor position. This high-level analog output was then connected to the first data acquisition system. Strain gages applied to the specimen were

connected to the individual strain gage conditioners. The conditioners supplied 2 V to the quarter bridge, and the return signal was filtered internally and then amplified to provide a high-level ($\pm 10 \text{ V} = \pm 50,000$ microstrain) signal proportional to the amount of specimen strain, and that output was then connected to the second data acquisition system. For tests conducted at sub-ambient temperatures ($-20 \text{ }^\circ\text{C}$ and $-40 \text{ }^\circ\text{C}$), ten thermocouples were connected to the thermocouple data acquisition system. All three data acquisition systems were connected to a laboratory computer for digitization and data storage. The software used to digitize and store the data was a commercially available package designed to allow users to create custom acquisition and data analysis programs. The load, actuator displacement (stroke) and CMOD signals from the system controller were all supplied to the primary data acquisition system. The secondary data acquisition system was integral to the test-frame controller. A custom test program was written to accommodate both frame control and data acquisition. The channel count was a limiting factor for the secondary data acquisition system, and therefore it was used only as a back-up system to acquire the most critical test data, namely the load, stroke, CMOD and LVDT data.

The data acquisition rate for both systems was 20 Hz. The data flow and connection diagram are shown in Figure 20. The primary data acquisition system captured the following data:

- time
- force
- stroke
- CMOD gauge
- left CMOD gauge (not used on all tests)
- right CMOD gauge (not used on all tests)
- LVDT 1A: outside diameter – upper plate
- LVDT 1B: outside diameter – lower plate
- LVDT 2A: inside diameter – upper plate
- LVDT 2B: outside diameter – lower plate
- LVDT 3A: left spanning LVDT from OD view
- LVDT 3B: right spanning LVDT from OD view
- Strain gages 1-30: odd-numbered channels were transversely mounted and even-numbered channels were axially mounted gages
- Thermocouples 1- 10: channels 1-5 were mounted from top to bottom on the ID of the specimen and channels 6-10 were mounted from top to bottom on the OD of the specimen.

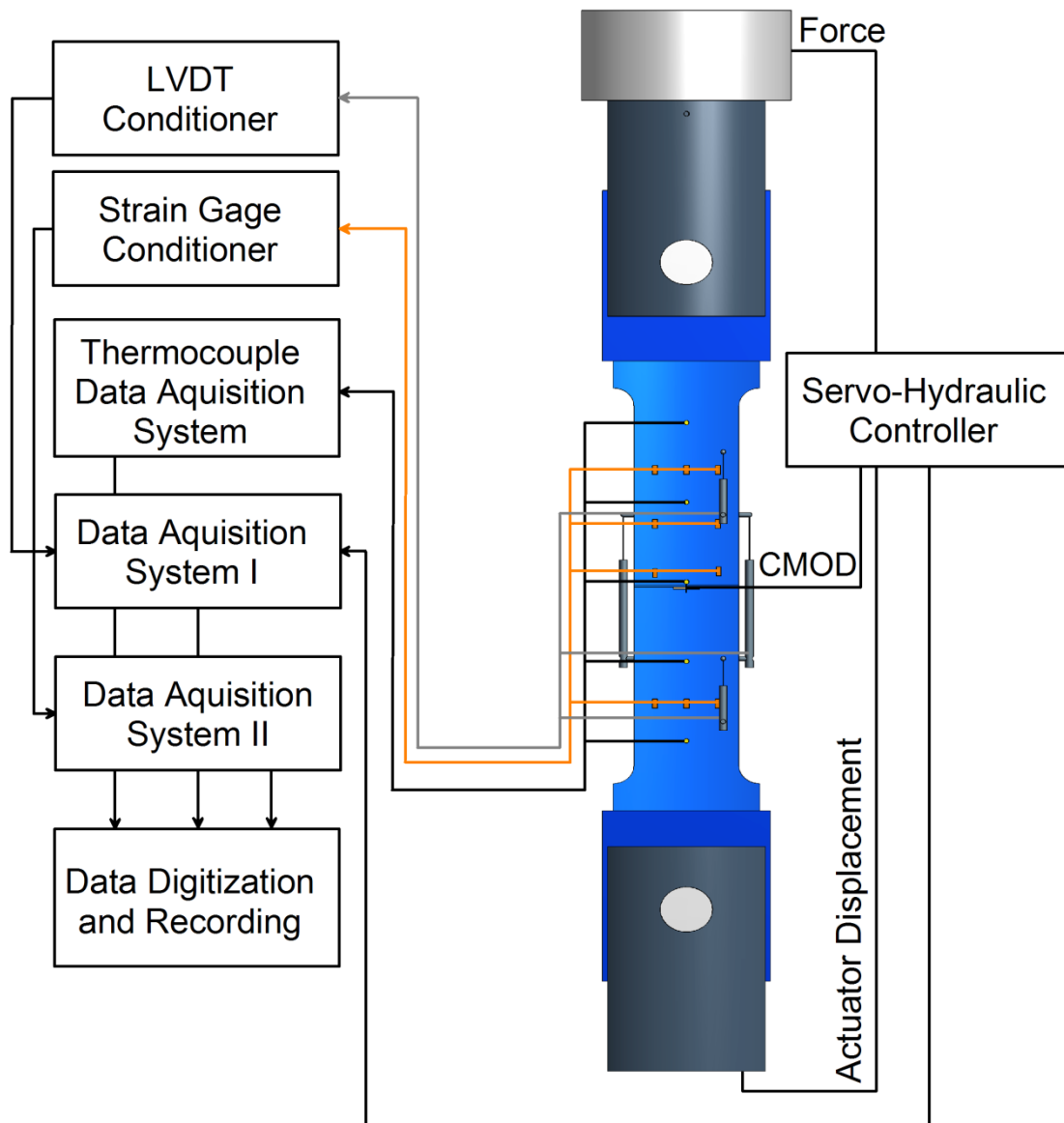


Figure 20. Schematic of the data flow and connection diagram for the CWP tests.

The primary data acquisition system recorded the signals in raw voltage. Conversion factors for engineering units were provided in each of the data headers. The data acquisition program on the servohydraulic controller recorded the data channels directly in engineering units. The following channels were captured by the secondary data acquisition system:

- time
- stroke
- center CMOD gauge
- left CMOD gauge (not used on all tests)
- Right CMOD Gage (not used on all tests)
- LVDT 1A: outside diameter – upper plate

- LVDT 1B: outside diameter – lower plate
- LVDT 2A: inside diameter – upper plate
- LVDT 2B: inside diameter – upper plate (not on all tests)
- LVDT 3A: left spanning LVDT from OD view
- LVDT 3B: right spanning LVDT from OD view.

There were not enough input channels on the controller to accept all the LVDT signals when the left and right CMOD gauges were used. When symmetry was demonstrated with the three CMOD gauges, one of those input channels was converted to accept signals from LVDT 2B.

5 TEST EQUIPMENT

5.1 LOAD FRAME

The load frame used at NIST is a fixed upper-crosshead, bottom-actuated servohydraulic system. The frame and actuator are force-rated to 4.45 MN (1 Mlb) in tension. The actuator is capable of 4.88 in (127 mm) stroke. The upper crosshead is fixed only when a test is being conducted. The upper crosshead height (distance between grips) can be adjusted by the screw-driven lifts. The large force capacity and physical dimensions of a frame such as this is required for testing specimens of this scale.

5.1.1 Load Measurement

The load measurement is taken from the servohydraulic control system, which is connected to a quad bridge canister-style force transducer rated for 4.45 MN (1 Mlb). The load cell is connected to the fixed upper crosshead and is coaxial with the clevis grips and the load line of the specimen. For this test program the servohydraulic controller was tuned for force control, as was necessary for preloading the specimen and maintaining that load during the cooling cycle of the sub-ambient temperature tests.

5.1.2 Stroke Measurement

The stroke (actuator movement) measurement is taken from the servo-hydraulic control system, which is connected to an LVDT. The LVDT is directly connected to the bottom clevis grip and gives an accurate record of actuator/grip position. The servo-hydraulic controller was also tuned for stroke control, as was necessary for the test profile detailed in Section 6.5.

5.2 SPECIMEN GRIPS

Two clevis grips were machined from 4340 steel. The clevis grips are attached to the actuator and the load cell with a single centered threaded adapter. Each clevis accommodates a 5 in (127 mm) diameter hardened steel pin. The clevis grips allow much easier installation of a specimen for a specimen of this size. The clevis grips allow one degree of rotational freedom about the pins. A photograph of the installed load cell, clevis grips and calibration block is shown in Figure 19.

5.3 ENVIRONMENTAL CHAMBER

A custom-designed environmental chamber was purchased for this test program. The chamber is capable of maintaining temperatures between -60 °C and 250 °C. For sub-ambient temperatures, the chamber is connected to a liquid-nitrogen dewar. The chamber has an opening on the top and

bottom to accommodate the specimen. It is also open in the “front” to allow the chamber to slide into place after the specimen is installed in the test frame. The clevis grips are outside the environmental chamber. Figure 21 shows a photograph of the test frame with a specimen installed and the environmental chamber emplaced, but with the door open. The chamber was supported by rollers that tracked on an aluminum frame that kept the chamber on the test frame while the specimen was being installed or removed from the frame. This access also allowed access to the instrumentation installed on the specimen prior to testing. The grips and end-tabs presented a significant source of heat for the specimen during sub-ambient testing. To ameliorate the heating effects of the grips and end-tabs, an actively cooled heat-exchange system was installed on the specimen near the end-tabs but inside the environmental chamber. The cooling blocks were made of copper and were interconnected by copper tubing, through which liquid nitrogen flowed during the cooling cycle as well as during the test. The top and bottom cooling systems were controlled independent of the environmental chamber and of each making it possible to finely control the temperature profile of the entire gauge section of the specimen. Figure 22 is a photograph of the cooling system installed on a representative CWP specimen. Copper-laden thermal-transfer grease was used to couple the specimen to the cooling system. The cooling blocks were installed on the OD surface of the specimen after it was installed in the test frame.

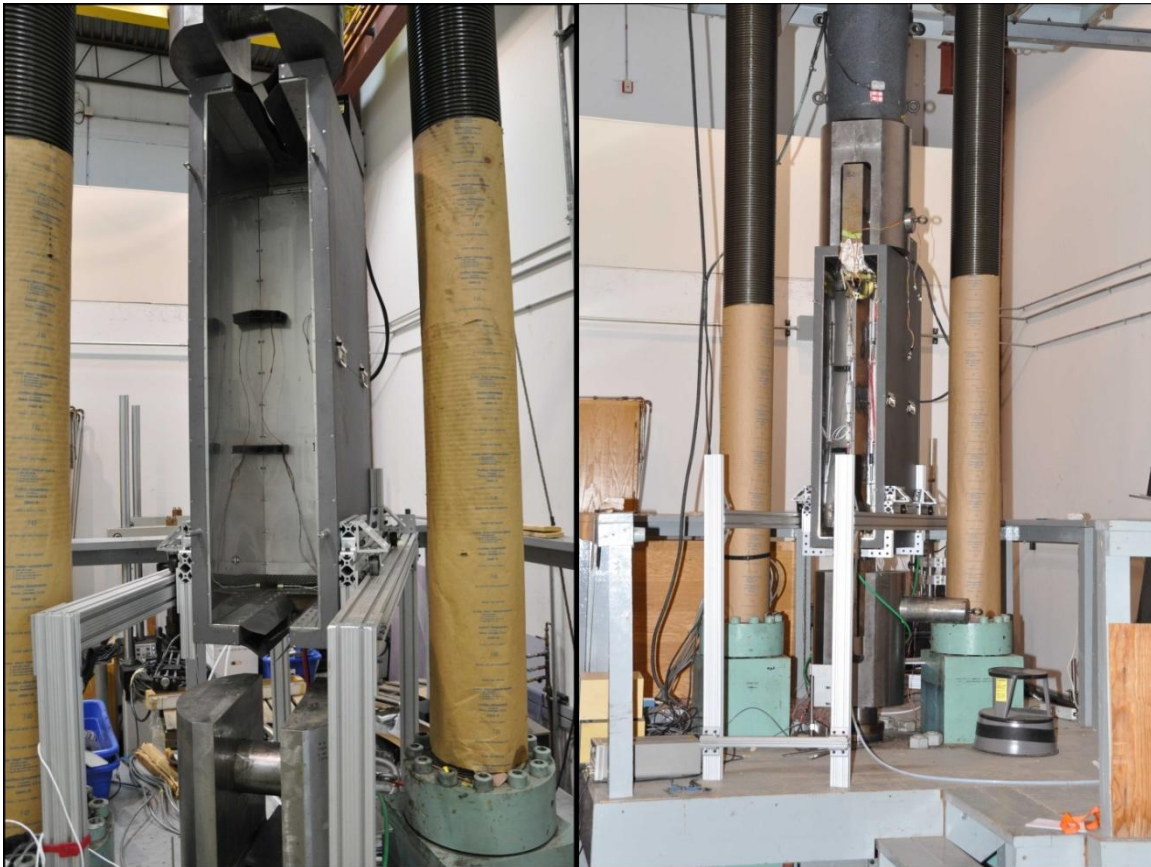


Figure 21. The empty environmental chamber (left) and an installed CWP specimen, with the environmental chamber between the grips prepared for testing (right). The chamber is supported by rollers attached to a

tracked aluminum frame, allowing the chamber to easily slide in and out of the way of the load line of the frame.



Figure 22. Bottom cooling blocks installed on a CWP specimen.

6 TEST PROCEDURE

6.1 PHYSICAL MEASUREMENTS

Several standard physical measurements were made prior to testing on each CWP specimen. These include specimen gauge length, LVDT spacing, plate thickness, arc length, and chord gauge width. The gauge length was measured with a measuring tape with a minimum dimensional increment of 1 mm. The measurement was made from the tangent points between the fillets on either side of the reduced gauge section of the test specimen. The initial spacing of

the LVDT attachment studs for each LVDT was measured to provide an initial length for strain measurement. The LVDT initial spacing measurements were made with a digital caliper having 20 μm resolution. The specimen thickness was measured at the edge of the plate on the top side of the weld with a micrometer that had spherical anvil caps and 2 μm resolution. The arc length was measured by placing a thin, flexible steel machinist's ruler along the concave arc of the ID surface, aligning the edge of the ruler to the edge of the specimen. The machinist's ruler had minimum dimensional increments of 0.5 mm. The chord gauge width was measured between the machined edges of the specimen with a digital caliper with a 20 μm resolution.

6.2 SPECIMEN INSTALLATION

The CWP specimens tested in this project weighed in excess of 340 kg (750 lb). Each specimen was 2.1 m (84 in) long, which presented unique handling challenges. An overhead crane was used to move specimens around the laboratory and prepare them for installation after all the instrumentation was applied to the specimens, except for the CMOD gauge and LVDTs. Once the specimen was vertical, it was supported against the test frame and then lifted and moved by use of the overhead crane outfitted with an adjustable counter-balance strong-back. The specimen was first inserted into the upper clevis, and the clevis pin was then installed. Figure 23 is a photograph taken during specimen installation of a representative specimen. Once the pin was installed, the weight of the specimen was on the clevis pin, and the counter-weight system was removed for testing.

Shims were installed over the clevis pin, between the end-tabs and the inside surface of the clevis grip. The shim thickness was determined by the centroid location of the gauge section to ensure that the centroid was coaxial with the load line of the test frame. Once the correct shim distance was set on the ID side of the specimen, filler shims were placed on the OD side of the specimen to effectively lock it in place and prevent the specimen from moving out of alignment during loading.



Figure 23. Photograph taken during the specimen installation process. The movable counter-balance strong-back was supported by the overhead crane, allowing adequate reach into the test frame, where the overhead crane had no direct access, because of the crosshead.

6.3 INSTRUMENTATION PREPARATIONS

Once the specimen was hung, the remainder of instrumentation was installed. The LVDTs were secured to their respective mounting studs, and all the wire bundles were routed to the edge of the specimen and down to the platform, where they were connected to their respective conditioners. All strain gages were connected to the break-out boxes. Each gage was then shorted at the terminal strips on the specimen to verify the correct channel connections. The strain gage conditioners were zeroed, balanced and then shunt-calibrated. The LVDTs were all connected to their conditioners, and the signals were zeroed.

The bottom clevis was moved into place with the actuator, and the pin was inserted through the bottom end-tab. Shims were installed in the bottom clevis to maintain the same alignment as was achieved in the upper clevis. The actuator was then moved to make contact with the lower clevis pin. Any load applied to the specimen was removed, and the load and stroke signals were zeroed. The CMOD gauge was installed in the notch, and the spring retainer was installed to prevent the clip gauge from moving during the test. The CMOD signal was zeroed.

The data acquisition systems were prepared with actual specimen measurement data to be included automatically in the raw data file header. Each strain gage was shunt calibrated and adjusted and re-zeroed. A calibration verification data file was generated by running the data acquisition system and performing the shunt-calibration switching while running. This calibration verification file was useful post-test to diagnose data channel problems if any were encountered during the test. This file was also used to determine the noise floor of the signals, thereby recording the uncertainty of the signals due to natural electrical interference.

6.4 PRE-LOAD

A pre-load of 13.3 kN (3000 lb) was applied to each specimen prior to testing. The pre-load was maintained in load control until the test began. For sub-ambient temperature tests, this load control allowed the actuator to move to adjust for specimen response (shrinkage) during the cooling cycle while maintaining a constant load on the specimen.

6.5 COOLING

Twenty-three of the 34 specimens were tested at either -20 °C (17 specimens) or -40 °C (6 specimens). Cooling the specimens was achieved with liquid nitrogen metered into the environmental chamber and was controlled by the chamber's PID (proportional - integral - derivative) controller. The chamber used an integral thermocouple that was not connected to the specimen. A cooling data set was collected on the primary data acquisition system to record the signal responses to the temperature change as well as the ten thermocouples during the cooling cycle. A cooling rate was not specified; however, post-test analysis of the cooling data showed that most specimens were cooled at an average rate of 1 °C/min. More important was to control the upper and lower cooling blocks to maintain a temperature differential between all ten thermocouples to within ± 3 °C. Maintaining this differential during the cooling cycle made it much easier to maintain that differential during the hold/soak period and throughout the duration of the test.

6.6 TEST EXECUTION

Room-temperature tests and sub-ambient temperature tests on specimens were conducted the same way for all the specimens, after the temperature had stabilized. All nonessential personnel were cleared from the lab. The control system was taken out of manual load control, and control was then transferred to the test profile programmed for this test. The data acquisition system and the test profile were started. All signals were monitored during the test to ensure that the sensors were operating correctly. Sensors that failed during the test were evaluated and if determined to be critical to continuation, the test was stopped and the problem was corrected. If they were determined to be non-critical, the test was allowed to continue. An example of a critical signal is the CMOD, and an example of a non-critical signal is a thermocouple or a strain gage. This determination also depended on when during the test the signal was lost. For instance, the test

was stopped for most channels early in the elastic loading part of the test, since there was little consequence to stopping the test to diagnose and possibly repair the issue.

6.6.1 Loading Profile

The loading profile of this test program mimicked that of a traditional small-scale fracture toughness test. The goal of the loading profile was to acquire unloading and loading compliance data throughout the test, which would be used to determine the instantaneous crack depth. The specimens were loaded in tension at a stroke-controlled rate of 6.00 mm/min. Specimens were loaded in the elastic regime with a minimum of six unloading cycles. Load limits were used to trigger the unloading and loading ramps. The upper triggers incremented by 222.4 kN and the lower load triggers were 20 % of the upper trigger. Past the yield point, the program shifted to stroke-limited upper triggers. The specimens were unloaded in stroke control by 889.6 kN with load signal thresholds and then reloaded 800.7 kN, at which point the stroke limit (2.0 mm) was again in effect. This cycle was repeated until one of several end-of test conditions was met. Figure 24 is a graphic representation of this unloading and reloading cycle.

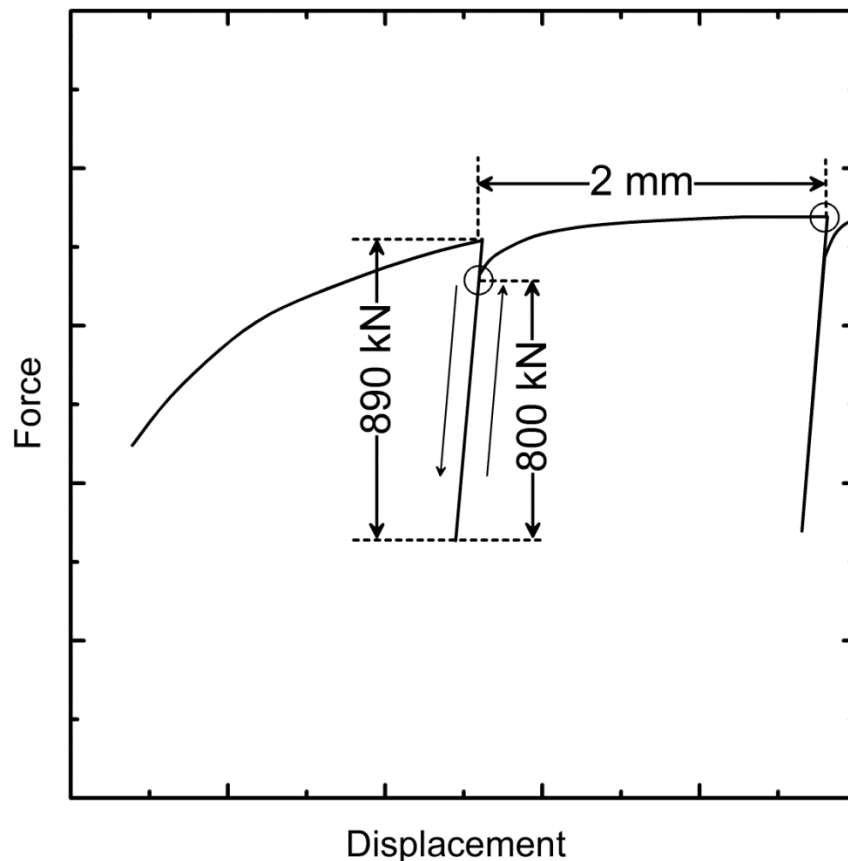


Figure 24. Graphical representation of the unloading and reloading triggers used after the yield point in the test. The circles represent the areas where the limits switch from load limits to displacement limits (left circle) and then back (right circle).

6.6.2 End-of-Test Determination

One goal of this test was to capture the onset of ductile tearing and then evaluate the ductile tearing characteristics. It was desired to continue all the tests past the obvious maximum load. Most of the specimens had a very flat “load vs. CMOD” or “load vs. stroke” plot at or near the

maximum load, making it very difficult to determine whether the maximum load had been reached, given the amount of signal uncertainty in the load signal. The tests were programmed to stop automatically if the load dropped below 80 % of the specimen UTS after the UTS had been reached. A manual stop condition was also provided to the test operator monitoring the CMOD vs. stroke plot. As this real-time plot approached a vertical asymptote, it was apparent that very little stroke was necessary for large increases in the CMOD signal, indicating gross tearing and approaching the point of unstable collapse. The test was ended before complete specimen rupture for all but two specimens. The two that failed were unexpected and ultimately resulted in an improvement in the end-of-test criteria, namely, the close monitoring of “CMOD vs. stroke” data. Figure 25 shows a plot of data representative of many CWP tests. This specimen failed unexpectedly. It is clear in the plot that the CMOD data reached a vertical asymptote, however these data were not monitored during the test. Real-time monitoring of “CMOD vs. stroke” data immediately became part of the procedure after this specimen failed.

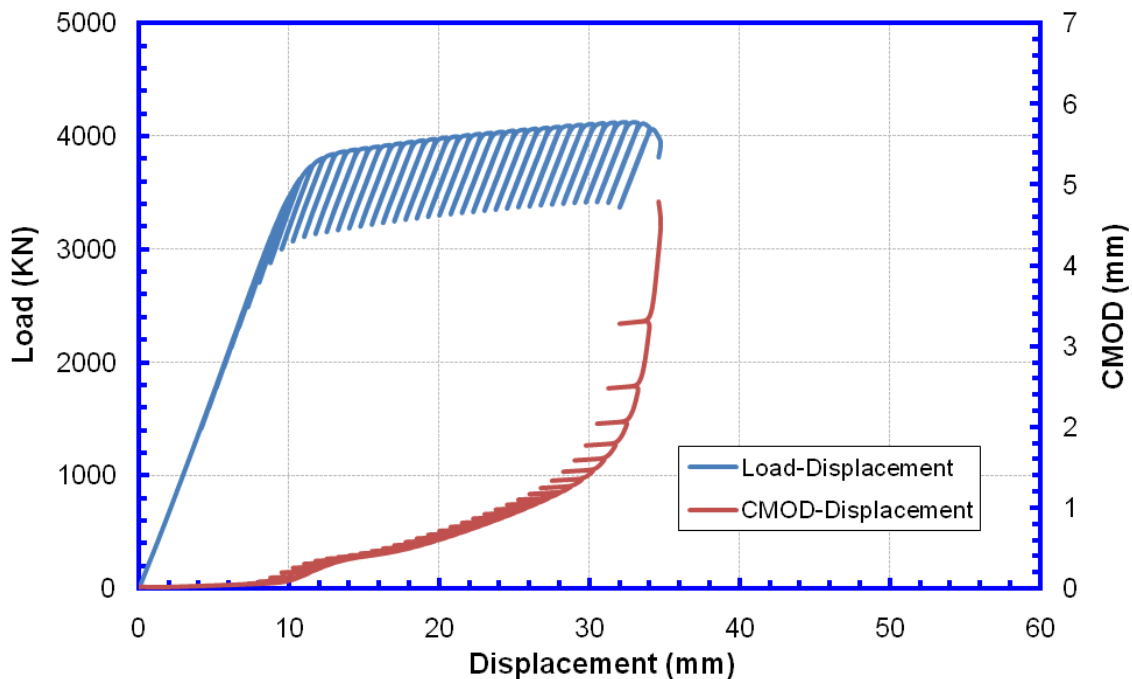


Figure 25. Load-displacement and CMOD-displacement relation (Specimen ID: CWP-11)

6.7 POST-TEST ACTIVITIES

As soon as the test was complete, the actuator was moved in order to allow removal of the lower clevis pin, and the hydraulic system was shut down. The data were backed up to a NIST server and the data verification was begun. The specimen was allowed to warm in the case of sub-ambient temperature tests and was removed from the test frame to be sectioned for post-test analysis.

6.7.1 Environmental

Sub-ambient temperature tests presented a challenge to protect the newly formed fracture surfaces. If the chamber was removed immediately, water vapor would condense on the surface and would result in rust on the fracture surfaces. To avoid this, specimens were allowed to warm in the chamber at a natural rate, thus eliminating the possibility of condensation on the surface.

The turnaround period between sub-ambient temperature tests could be improved by programming the chamber controller to warm the specimen with internal heaters, allowing for acceleration of the test schedule. Once the specimen and chamber were at ambient temperature, the chamber was removed from the specimen, the active cooling blocks were removed, and specimen removal was possible.

6.7.2 Specimen Removal

Instrumentation was disconnected in the opposite order of how the specimen was prepared for testing. Wire bundles were carefully labeled for particular instruments so that the wires could be re-used on future specimens. The specimens were removed in reverse order of the installation procedure with the strong-back and over-head crane.

6.7.3 Gross Sectioning

The end-tabs were cut from each of the specimens with a metal-cutting circular saw. The specimen was then sectioned to separate all but the area surrounding the weld and fracture. The remaining section was approximately 254 mm (10 in) square. The sectioning was performed on a very large band saw. Other saw-cuts were made to allow easy access to the failure surface for post-test analysis. The sectioning schematic in Figure 26 illustrates where saw-cuts were made to obtain the overall shape of the section in preparation for EDM sectioning.

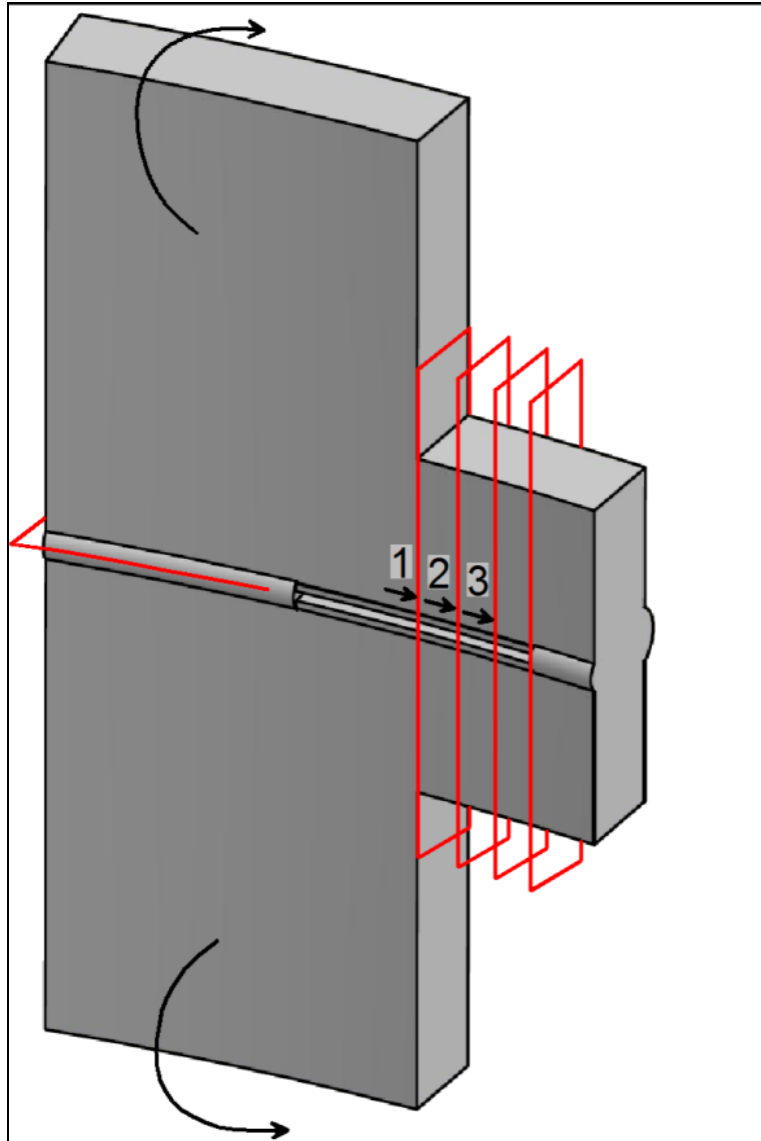


Figure 26. Schematic of a sectioned specimen after testing. The vertical sectioning planes shown in red are for EDM slicing. The horizontal sectioning plane was back cut with a band saw to make it easier to liberate the fracture surface in three-point bending.

7 SPECIMEN ANALYSIS

7.1 DATA VERIFICATION

Raw data files collected from each test were evaluated to determine whether the data set was valid. The first verification was a complete data set to explain anomalies such as dropped channels. Second, the raw-data scaling for engineering unit conversions was verified.

Validated data files were compressed and uploaded to the CRES file transfer protocol (FTP) site. Data files were archived on a NIST server and removed from the test computers. Incomplete data records or channels with data loss were examined to determine the cause of the data acquisition problem. Some tests had channels dropout as the test progressed; for example, strain

gages failing, thermocouples failing or the CMOD gage popping out of the notch on early tests caused a loss of valid data. These issues were noted for each data set, and when necessary and possible, the data set was corrected.

7.2 RESIDUAL FLAW GEOMETRY

After the test was complete, the flaws had residual shape resulting from the plastic deformation around the initial notch location. The residual flaw geometry was determined for each specimen with a variety of techniques. Each technique was calibrated to ultimately allow accurate geometrical dimensions of the residual flaw to be obtained.

When the technology became available to NIST, a three-dimensional (3D) laser scanner was used to obtain a surface mesh file of the notch location on the inside and outside diameter of the specimen section. As part of the original scope of work, crack-mouth profiles were obtained from optical photographs of the crack mouth. Figure 26 shows how the fracture surfaces were sectioned and viewed after laser scans and crack-mouth profiles were obtained. Fracture surface photography (fractography) was performed on each of the specimens for optical verification of the initial and final flaw dimensions. Also seen in Figure 26 are three surface planes that identify how the cross-sectional views were obtained and in what direction they are viewed.

The details of the sectioning and the processes were not completely known at the beginning of the program, and some specimens were sectioned slightly differently from others. By the end of the test program, a consistent methodology was used and is presented in the following paragraphs.

7.2.1 Laser Scans

A 3D laser scanner was used to document the fracture surface and to obtain a 3D model of the notch area of the specimen. The models capture the thinning that occurred surrounding the notch location. This technology was not initially available to the program, and although each specimen was scanned, a complete analysis has not been conducted on the scans. The scans and a discussion of the useful data obtained from the scans will be included in a report addendum when the analysis is complete.

7.2.2 Crack Mouth Profile

Optical photography of the residual crack mouth was performed on each specimen. The post-test residual crack mouth profile provides an indication of the plastic deformation surrounding the flaw. Each specimen was photographed with a consistent set-up and calibration so that measurements from the photographs, and therefore direct comparisons between specimens, could be made. Crack-mouth profiles have been photographed and archived. Complete analysis of the photographs has not been completed and will be included in a report addendum when the analysis is complete. Figure 27 is a representative picture of a residual crack-mouth profile. From this photo the profile can be mapped and the dimension (x-y) data tabulated.

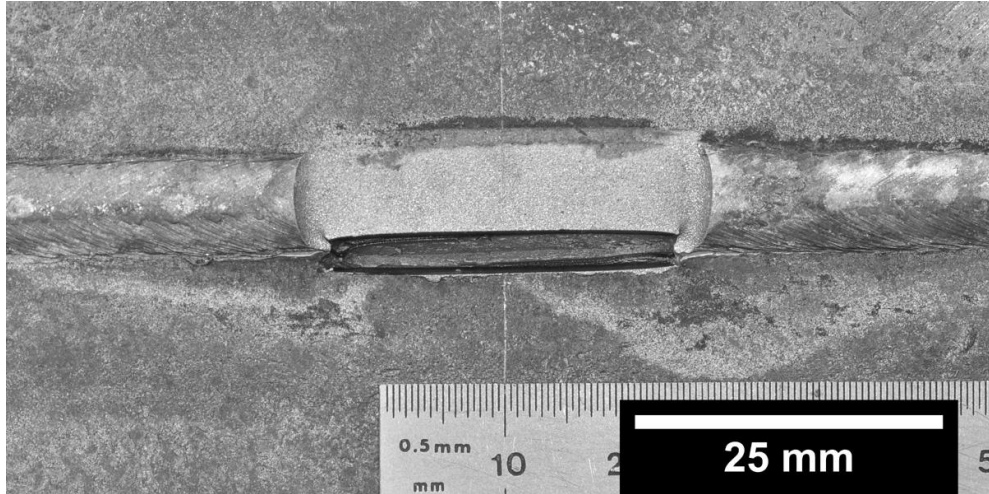


Figure 27. Photographs of the crack mouth profile were taken of each specimen to map the profile and quantify the residual opening. This example is from specimen CWP-12.

7.2.3 Fractography

Optical fractography was performed on each of the liberated fracture surfaces. From these fractographs, the initial crack depth a_o was measured. The final flaw geometry, including the final crack depth a_f , was also measured and recorded from these fractographs. These data are provided in Table 7. Fracture surfaces were liberated by saw-cutting most of the remaining ligament, then cooling in a dewar of liquid-nitrogen, followed immediately by loading the specimen in three-point bending to break the remaining ligament.

Figure 28 is a representative fractograph. From this photo, the initial crack depth, final crack depth and general geometry of the crack front can be measured.

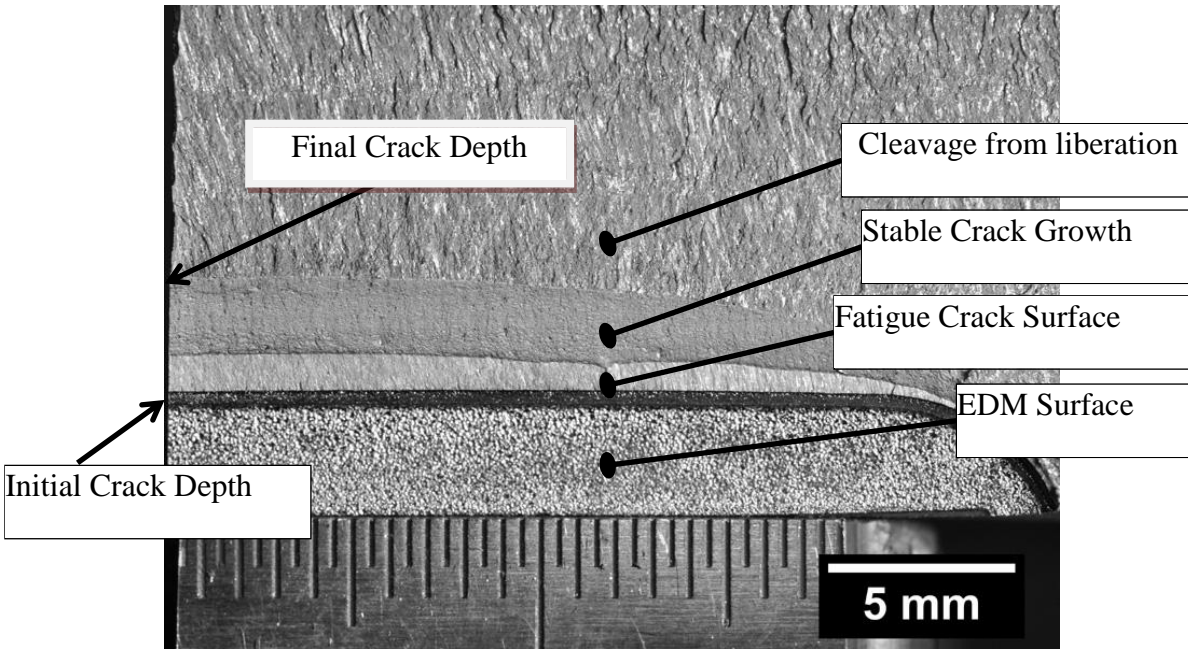


Figure 28. Fractographs of each specimen were taken to measure the initial and final crack depths, and to determine the crack propagation shape. This example is from specimen CWP-19.

Since this test program developed the fatigue pre-cracking method with the use of base metal specimens to calibrate the predictions, it was useful to learn from the fractographs how well the method worked for notches in the WMC and HAZ. Figure 29 shows the measured initial crack depth vs. the predicted initial crack depth for all CWP specimens. The solid line is the desired 1:1 line, and the dashed lines represent the ± 0.25 mm deviation from the 1:1 relationship. Most of the measured cracks fell within ± 0.25 mm of the predicted value; some of the error presented here is due to the difficulty in measuring the crack depths in the fractographs in addition to difficulty in accurately measuring the starting initial crack depth value a_0 . The crack-depths were measured from the mid-line section of the flaw (far left of the photograph). The surface adjacent to the steel scale in the photo was the datum for pixel count measurements up to the demarcations in the photograph. High-resolution photography was used in order to have a resolution better than 1 μm per pixel measured.

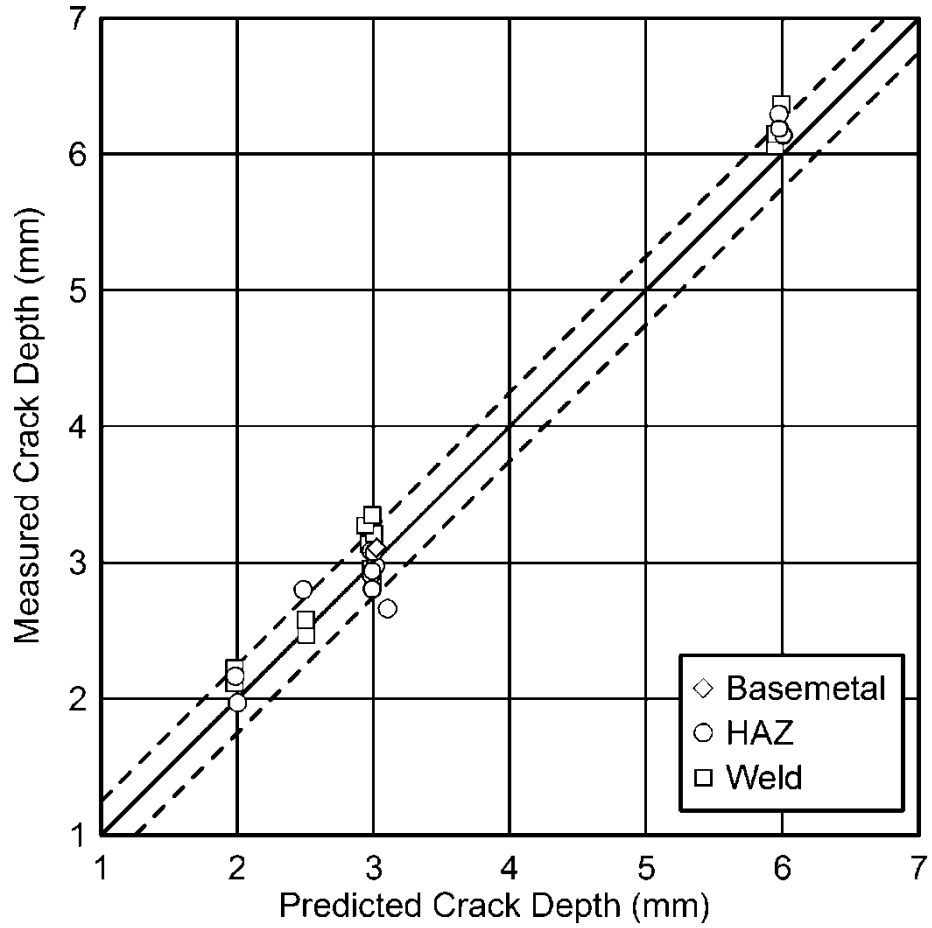


Figure 29. Measured crack depth vs. predicted initial crack depth for all CWP specimens. The data show an excellent predictive capability in the fatigue pre-cracking procedure. The tolerance bands represent an error of ± 0.25 mm.

Table 8. Measurements from fractographs

Specimen	Notch Location	Height Difference from EDM Notch Surface to Lower Plate ID Surface (mm)	Measured Notch Depth (mm)	Predicted Fatigue Pre-crack Depth (mm)	Measured Fatigue Pre-crack Depth (mm)	Final Crack Depth (mm)
CWP-BM-	BM	0.00	2.72			11.40
CWP-BM-	BM	0.00	2.30	3.02	3.11	4.44
CWP-2	HAZ	0.00	2.33	3.01	2.98	4.77
CWP-3	HAZ	0.21	2.78			9.02
CWP-5	HAZ	0.41	2.33	2.98	2.91	3.87
CWP-8	HAZ	0.21	1.36	1.99	2.17	3.06
CWP-9	HAZ	0.00	1.30	2.00	1.97	2.61
CWP-12	HAZ	0.63	5.20	6.00	6.14	7.96
CWP-15	HAZ	1.26	6.02			12.08
CWP-17	HAZ	1.03	2.34	3.00	3.09	3.86
CWP-18	HAZ	0.80	2.16	2.99	2.81	3.66
CWP-21	HAZ	0.76	2.36	2.98	3.09	5.74
CWP-23	HAZ	0.72	2.31	2.99	2.94	6.42
CWP-25	HAZ	0.39	5.34	5.97	6.29	8.97
CWP-27	HAZ	0.07	5.29	5.98	6.19	9.07
CWP-29	HAZ	0.04	2.66	2.99	3.35	4.34
CWP-31	HAZ	0.00	1.99	2.48	2.80	4.27
CWP-32	HAZ	0.23	1.68	3.10	2.66	4.08
CWP-1	WMC	0.45	6.07			9.30
CWP-6	WMC	0.57	1.34	1.98	2.12	4.10
CWP-7	WMC	0.68	1.35	1.98	2.23	3.90
CWP-10	WMC	0.46	5.23	5.94	6.06	10.87
CWP-11	WMC	0.24	2.30	2.96	3.14	10.74
CWP-13	WMC	0.39	2.27	2.99	2.95	5.34
CWP-14	WMC	0.54	2.26	3.00	3.21	5.86
CWP-16	WMC	0.27	3.39			11.41
CWP-19	WMC	0.00	2.31	2.94	3.27	5.25
CWP-20	WMC	0.00	2.23	2.99	2.88	7.76
CWP-22	WMC	0.00	2.36	2.98	2.96	7.33
CWP-24	WMC	0.05	5.46	5.99	6.36	9.42
CWP-26	WMC	0.10	5.24	5.95	6.15	9.67
CWP-28	WMC	0.05	2.44	3.00	3.08	6.25
CWP-30	WMC	0.00	1.87	2.50	2.58	4.24
CWP-33	WMC	0.46	1.73	2.50	2.47	2.61

7.2.4 Metallography

Figure 26 depicts the sectioning plan and view of each metallographic specimen in this test program. Every specimen was sliced with an EDM wire. The sections were mounted and polished to 1 μm roughness and then etched to reveal the microstructure with a 2 % nital etching solution. Each mount was then examined with an optical microscope with two magnifications to accurately determine the location and shape of the notch, fatigue pre-crack and final crack shape. Each mount was also scanned on a high-resolution flat-bed scanner to obtain a macro-scale view of the specimen. From this view it was apparent where the notch was located with respect to the weld structure, and it also provided excellent evidence of the crack propagation direction.

The cross-section view of slice 1 (see Figure 26) coincides with the axial center of the specimen and flaw. This view is the most important one to discern the location and placement of the starter notch and to determine the final location of the fatigue pre-crack. Subsequent slices are viewed to determine the amount of deviation from the weld structure, specifically in the case of flaws designated for the HAZ.

Representative examples of the metallography are shown in Figure 30 and Figure 31.

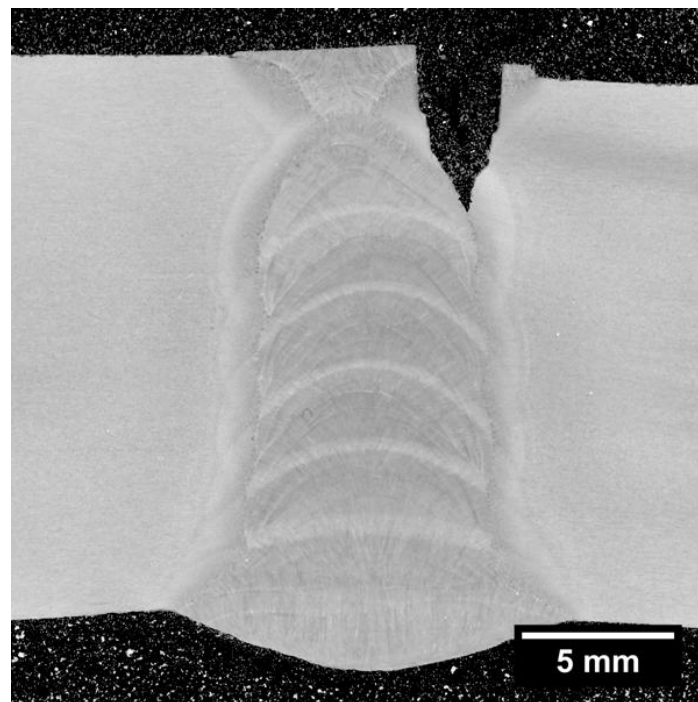


Figure 30. Metallography was performed on each specimen to document the location of the notch and pre-crack with respect to the weld structure. This macro-scale view was obtained with a high-resolution flat-bed scanner. This example is from specimen CWP-2.

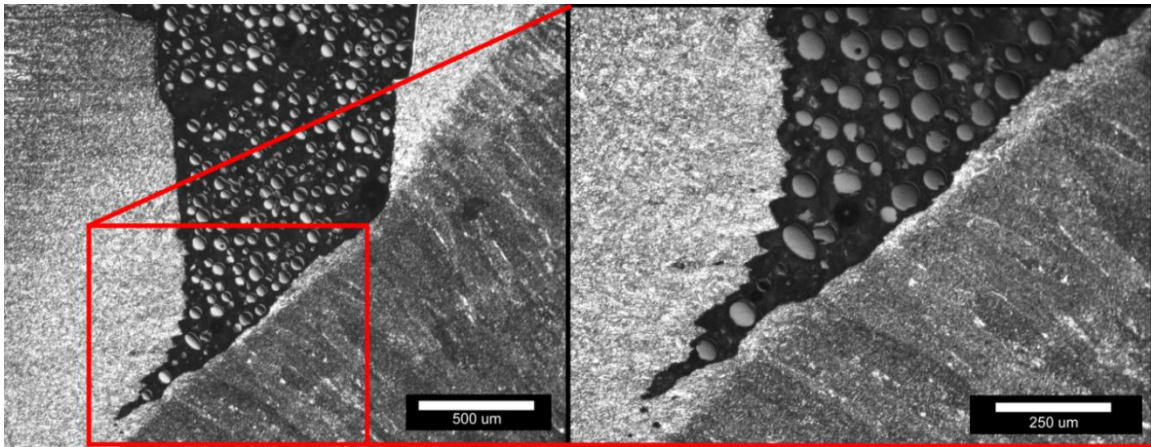


Figure 31. Metallography was performed on each specimen to document the location of the notch and pre-crack with respect to the weld structure. These low-power micrographs were obtained with a high-resolution CMOS camera attached to an optical microscope. This example is from specimen CWP-5.

At this point, the metallography has been completed for all specimens. Complete analysis on the photographs has not been completed and will be included in a report addendum when the analysis is complete.

7.3 SPECIMEN DISPOSITION

The fracture surfaces of all specimens have been preserved for future analysis if necessary. The metallographic mounts have also been archived for future analysis if necessary. The remaining steel from each specimen has been discarded for steel recycling.

8 DISCUSSION

8.1 TOPICAL REPORT COMPLETION

An enormous volume of data was generated in this test program. The critical data have been supplied to project collaborators and reported in another topical report [14]. Additional analysis of the strain fields, laser scans, crack mouth profiles and metallographic images is ongoing and the results are not yet available. An addendum to this report will include an analysis of those results and a discussion will be given that specifically addresses the interactions of the items noted in Section 2.1. For the purpose of this report, a discussion based on the data obtained and analyzed will be given in the next section.

8.2 DISCUSSIONS

Measurement techniques for this scale of testing and specifically for this scale of specimen are very complex and were developed and perfected to reduce overall uncertainty in the test program. The few anomalies which were encountered with respect to data sets will receive special attention in the next section. With in-house metallographic equipment and expertise, NIST was able to complete the fractography and metallography to demonstrate the accuracy of the pre-cracking procedure and to also document the crack propagation behavior of the flaws. The program presented many challenges that included budgets, schedules and, more importantly, technical challenges that can be expected from any large test program where standards are noticeably absent. This test program will certainly add to the knowledge base necessary for

comprehensive standardization of the CWP test. This is discussed in Section 8.4. These tests and results can be summarized by the following:

- Thirty-four medium-scale curved-wide-plate (CWP) tests were conducted at NIST.
- The CWP tests were successfully conducted at ambient and sub-ambient temperatures.
- The test program evaluated the effects of temperature, specimen geometry, flaw geometry and flaw location on the fracture resistance of girth welded X100 linepipe.
- The test program collected data allowing investigators to comprehensively evaluate the remote strain response in the specimens. Full analysis is ongoing.
- The test program comprehensively evaluated the fracture surfaces and crack propagation in the specimens, and full analysis is ongoing.
- It is possible to obtain highly consistent data from multiple sources, permitting detailed representation of the deformation of CWP specimens.
- The remote strains obtained from the regions above and below the girth weld were different, sometimes by a large amount. The difference in applied stress in those regions was minimal. The difference in strains was attributed to slight variations in material properties [15].
- Once the flaw growth starts to accelerate, the remaining additional strain capacity was limited.
- Considerable skill and care is needed in the instrumentation of the specimens and data interpretation to generate reliable resistance curves.

8.3 ANOMALIES

The test program reported here began with a liberal scope, allowing flexibility to conduct side experiments along the way to reduce the uncertainty and improve the overall efficiency of testing at this scale. Some techniques were modified along the way in response to anomalies and challenges faced in the program. For example, photoelastic techniques were an excellent tool to visually document the strain field in the specimen under loading conditions. However, consistent application of the photoelastic sheets was nearly impossible, forcing much iteration to be required in order to improve the technique. Furthermore, the photoelastic sheets complicated the installation of the strain gages and LVDTs.

CMOD gauges were initially installed in the notch with just the spring force of the gauge to keep them installed. This proved to be problematic, as clip gauges popped out of the notch on several occasions during the testing of a couple of specimens. When this occurred, the systems were paused and the CMOD gauges were replaced. However, they did not always return to the previous value, making it difficult to correct the data by time alone. In order to facilitate automatic data processing and analysis, the data sets needed corrections in the CMOD signal and not just the time delay. CMOD data were critical to the program, so great attention was given to ensuring the fidelity of the CMOD data.

Some strain gages did not last the entire test. This was attributed to installation imperfections. Data from an individual strain gage was not critical to the outcome of every test. Sufficient data are available to perform an adequate analysis of the strain field in the specimen under loading conditions.

Metallographic mounts were difficult to prepare for specimens that ruptured during the test. Our best effort was given to re-align the specimen and obtain valid images.

As previously mentioned, not all laser scans and crack-mouth-profile photographs were performed on intact specimens. The procedures changed slightly as the program progressed. The final methodology has been reported here.

8.4 TEST METHOD STANDARDIZATION

One goal of this test program is to work toward a standardized test method. Drafting this method has begun but is not ready for review at this time. The remaining analyses must be performed on this program in order to allow complete understanding of interactions described in Section 2.1.

8.5 FUTURE WORK

Outstanding addenda described earlier are on-going and include a comprehensive examination of fractography and laser scans as well as data reduction on the strain gage data. The general considerations described in Section 2.1 will be discussed in detail when the additional analysis is complete.

Test-method standardization remains an outstanding goal of this program. It is anticipated that other research will be necessary after the final analyses are complete for the current work. For example, the effect of notch acuity and its interaction with temperature should still be explored. Conclusions found from analysis of the data by CRES suggest that further work is necessary to improve the unloading compliance measurement, because it is used directly to determine the flaw growth.

9 CONCLUSION

Considerable effort was given to the development of a CWP test process. The processes and details reported here are the results of several years of work. Some analysis of the data obtained remains outstanding; however, based on the reported results, it is clear that excellent data were obtained, and that a practical approach to the measurement challenges has been clearly defined for future work.

The establishment of the compliance function provides a convenient method for the calculation of flaw depth. It allows a quick and direct estimation of flaw depth from “CMOD vs. load,” which is measured in CWP tests. In addition, the capability of estimating the flaw depth establishes a necessary component for the construction of flaw-growth resistance curves. Given the flaw depth and length used in the finite element analysis, the applicable ranges of the compliance function are 0.0 mm to 12.0 mm for flaw depth and 30.0 mm to 75.0 mm for flaw length. Raw data obtained in this program was supplied to CRES for analysis. The high number of channels of various instruments allowed for the evaluation of several of the interactions that have been cited as necessary to fully understand a CWP test. Ultimately this is necessary for proper characterization of the fracture properties of the specimen, as it is compared to other tests of different scales. For the first time, a CWP test program has been evaluated as a potential fracture-mechanics test, useful in providing critical data needed in strain-based design of pipelines.

10 REFERENCES

- 1 Denys, R., "Weld Plate Testing of Weldments, Part I, II, and III, Fatigue and Fracture Testing of Weldments," ASTM STP 1058, pp. 157-228. ASTM, Philadelphia, 1990.
- 2 Denys, R., Lefevre, A. A., Glover, A., G., "Weld Metal Yield Strength Variability in Pipeline Girth-welds," Second Pipeline Technology Conference, Ostend, Belgium, Vol. II, pp.591-598, 1995.
- 3 Wang, Y.-Y., Liu, M., Stephens, M., Petersen, M., and Horsley, D., "Recent Developments in the Strain-Based Design of Pipelines," 17th Joint Technical Meeting of EPRG/PRCI/APIA, Milan, Italy, May 11-15, 2009.
- 4 Denys, R., Lefevre, A., and Baets, P. D., "A Rational Approach to Weld and Pipe Material Requirements for a Strain Based Pipeline Design," Proceedings of Applications & Evaluation of High-Grade Linepipes in Hostile Environments, Pacifico Yokohama, Japan, pp. 121-157, November 7-8, 2002.
- 5 Wang, Y.-Y., Liu, M., Chen, Y., and Horsley, D., "Effects of Geometry, Temperature, and Test Procedure on Reported Failure Strains from Simulated Wide Plate Tests," 6th International Pipeline Conference, Paper No. IPC2006-10497, September 25-29, Calgary, Alberta, Canada, 2006.
- 6 Wang, Y.-Y., Zhou, H., Tyson, W.R., Gianetto, J.A., Quintana, M.A., Weeks, T.S., "Curved Wide Plate Test Results and Transferability of Test Specimens", Final Report 277-T-11 to PHMSA per Agreement # DTPH56-07-T-000005, September 2011.
- 7 Panday, R. and Daniel, J., "Materials Selection, Welding And Weld Monitoring", Final Report 278-T-02 to PHMSA per Agreement # DTPH56-07-T-000005, September 2011.
- 8 Gianetto, J.A., Tyson, W.R., Park, D.Y., Shen, G., Lucon, E., Weeks, T.S., Quintana, M.A., Rajan, V.B. and Wang, Y.-Y., "Small Scale Tensile, Charpy V-Notch, and Fracture Toughness Tests", Final Report 277-T-05 to PHMSA per Agreement # DTPH56-07-T-000005, September 2011.
- 9 Richards, M.D., Weeks, T.S., McColskey, J.D., Wang, B., Wang, Y.-Y., "Fatigue Pre-Cracking Curved Wide Plates in Bending", 8th International Pipeline Conference, Paper No. IPC2010-34168, 2010, Calgary, Alberta, Canada, September 27 – October 1.
- 10 J.C. Newman and I.S. Raju, "Analyses of Surface Cracks in Finite Plates Under Tension or Bending Loads," NASA Technical Paper No. 1578, 1979.
- 11 ASTM Standard E1237, 1993 (2009), "Standard Guide for Installing Bonded Resistance Strain Gages," ASTM International, West Conshohocken, PA, 2009, DOI: 10.1520/E1237-93R09.
- 12 ASTM Standard E83, 2010a, "Standard Practice for Verification and Classification of Extensometer Systems," ASTM International, West Conshohocken, PA, 2009, DOI: 10.1520/E0083-10A.
- 13 ASTM Standard E2730, 2010, "Standard Practice for Calibration and Use of Thermocouple Reference Junction Probes in Evaluation of Electronic Reference Junction Compensation Circuits," ASTM International, West Conshohocken, PA, 2010, DOI: 10.1520/E2730-10.
- 14 Wang, Y.-Y., Zhou, H., Tyson, W.R., Gianetto, J.A., Quintana, M.A. and Weeks, T.S., "Curved Wide Plate Test Results and Transferability of Test Specimens", Final Report 277-T-11 to PHMSA per Agreement # DTPH56-07-T-000005, September 2011.
- 15 Wang, Y.-Y., Liu, M., Gianetto, J., and Tyson, B., "Considerations of Linepipe and Girth-weld Tensile Properties for Strain-Based Design of Pipelines," *Proceedings of the 8th International Pipeline Conference*, Paper No. IPC2010-31376, Calgary, Alberta, Canada, September 27 – October 1, 2010.